Technical Report

Numerical Hydrodynamic Modelling of the Tuna Farming Zone, Spencer Gulf

Mike Herzfeld, John F. Middleton, John R. Andrewartha, John Luick, Leeying Wu

March 2009

Aquafin CRC Project 4.6

(FRDC Project No.2005/059)

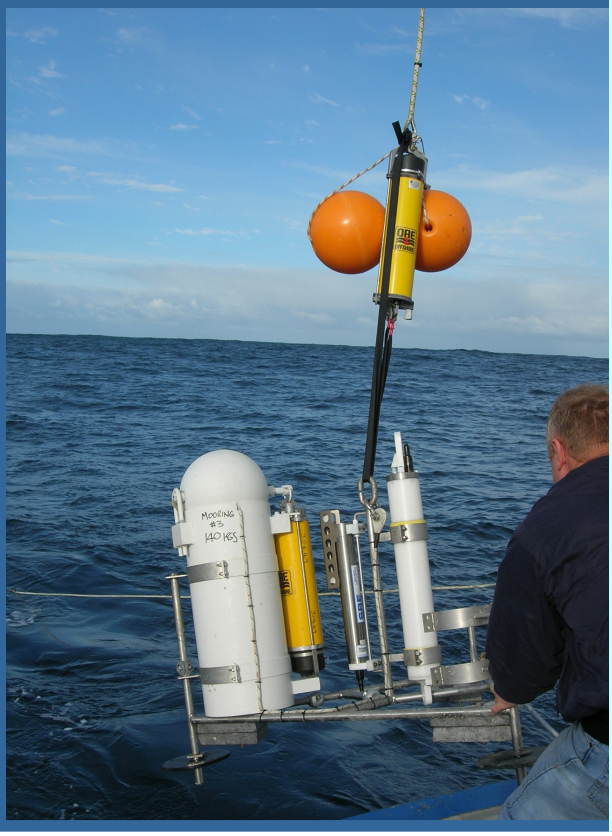

This publication may be cited as:
Herzfeld, M., Middleton, J.F., Andrewartha, J.R., Luick, J. and Wu, L. (2008) Numerical Hydrodynamic Modelling of the Tuna Farming Zone, Spencer Gulf. Technical report, Aquafin CRC Project 4.6, FRDC Project 2005/059. Aquafin CRC, Fisheries Research & Development Corporation and South Australian Research & Development Institute (Aquatic Sciences), Adelaide. SARDI Publication No F2008/000745-1, SARDI Research Report Series No 342, 100 pp.

Printed in Adelaide, March 2009
SARDI Aquatic Sciences
PO Box 120
Henley Beach SA 5022

SARDI Aquatic Sciences Publication Number F2008/000745-1
SARDI Research Report Series Number 342
ISBN Number 978-1-921563-11-9

Authors: Herzfeld, M., Middleton, J.F., Andrewartha, J.R., Luick, J. and Wu, L.
Reviewers: Paul van Ruth, Charles James
Approved by: Jason Tanner

Signed:
Date: 24 March 2009
Distribution: FRDC, ASBTIA, SARDI Aquatic Sciences Library
Circulation: Public domain

Numerical Hydrodynamic Modelling of the Tuna Farming Zone, Spencer Gulf

Mike Herzfeld[1], John F. Middleton[2], John R. Andrewartha[1], John Luick[2], Leeying Wu[2]

[1] CSIRO Marine and Atmospheric Research
Castray Esplanade
Hobart Tas 7000

[2] SARDI Aquatic Sciences
2 Hamra Ave
West Beach SA 5024

March 2009

Aquafin CRC Project 4.6

(FRDC Project No. 2005/059)

Table of Contents

List of tables

List of figures

Non-technical summary

A numerical hydrodynamic model was developed for the Spencer Gulf / Boston Bay region in order to investigate the circulation, flushing and connectivity of the region. The model also served as the driver for biogeochemical and sediment transport models, which were coupled to the hydrodynamic model. The model was forced with measured meteorological fields at the sea surface (wind, pressure, temperature) and sea surface elevation, temperature and salinity at the offshore boundary. The offshore boundary forcing was obtained using a nesting strategy involving a larger scale regional model.

The model output was compared to measured temperature and salinity data that was collected during a field program during 2005 / 2006. Sea level comparisons were also made with data measured at Port Lincoln, Wallaroo and Whyalla, and temperature, salinity and current comparisons were made with mooring derived data from the tuna farming zone (TFZ). Various model parameters and processes were optimized to achieve the best comparison between measured and modelled data. This optimization process provided insight into which parameters and processes the model was sensitive to. Simulations using the model were performed for the period August 2005 – August 2006, providing output of currents, sea level and temperature and salinity distributions.

The results from the data show there to be a strong (~20 cm s^{-1}) tidal currents that are very well reproduced by the model and that may be implicated in bottom stirring but not transport: particle displacements due to the tides were small and less than 1.4 km over a 3 hr period. Results for the weather-band currents (periods 3-20 days) are reasonably well produced by the model and show smaller currents (< 5 cm s^{-1}). However, due to the longer periods these can be important to the transport and flushing of the region: a 5 cm s^{-1} current with period 10 days will transport a fluid parcel 7 km over a 2.5 day period. Both data and model indicate the mean currents to be weak (~ 1 cm s^{-1}) and to the north/north east during both summer and winter: transport here over a 3-month period is around 80 km.

The gulf-scale model reproduces the clockwise circulation expected for winter. During summer, a similar pattern is found and opposite that expected from other studies. Nonetheless, the model does show predictive skill in the TFZ.

The currents were also found to be strongly sheared in the vertical and so may be important to shear enhanced diffusion and dispersal. However, estimates of the flushing times based on tracers and Lagrangian tracking show range from 10 days (Boston Bay) to 2 days (TFZ).

During summer, the model and data show a degree of connectivity between the coastal zone and the outer bay region that can be caused by local upwelling during summer, whereby offshore (eastward) winds force surface waters offshore, with onshore bottom flow. On the shelf, these winds would be downwelling favourable. In addition, the larger evaporation that occurs near the coast leads to dense water formation and bottom plumes that flow to the outer bay region. During winter, similar plumes result from coastal cooling rather than evaporation.

The strong seasonal cycle for temperature (salinity) is reproduced by the model to within1 ^{o}C (0.1 psu), and is shown to be largely driven by local heating (evaporation). Evidence does exist that local transport processes, including wind-driven upwelling and dense water formation, also effect temperature and salinity.

1. Background

Boston Bay is situated in the lower western side of Spencer Gulf (Figure 1.1) on the southern coast of Australia, and is the base for a large tuna aquaculture industry. This industry occupies the waters offshore of Boston Island, in an area hereafter called the tuna farming zone (TFZ). This area has been subject to detailed studies of the interactions between aquaculture and the environment. The present document is part of a larger study that seeks to develop an integrated hydrodynamic, sediment & biogeochemical model of the TFZ, to address environmental risks to the tuna industry, and to assess where nutrients released by the industry are dispersed to and what their potential environmental effects are. The larger study is detailed in Tanner and Volkman (2008).

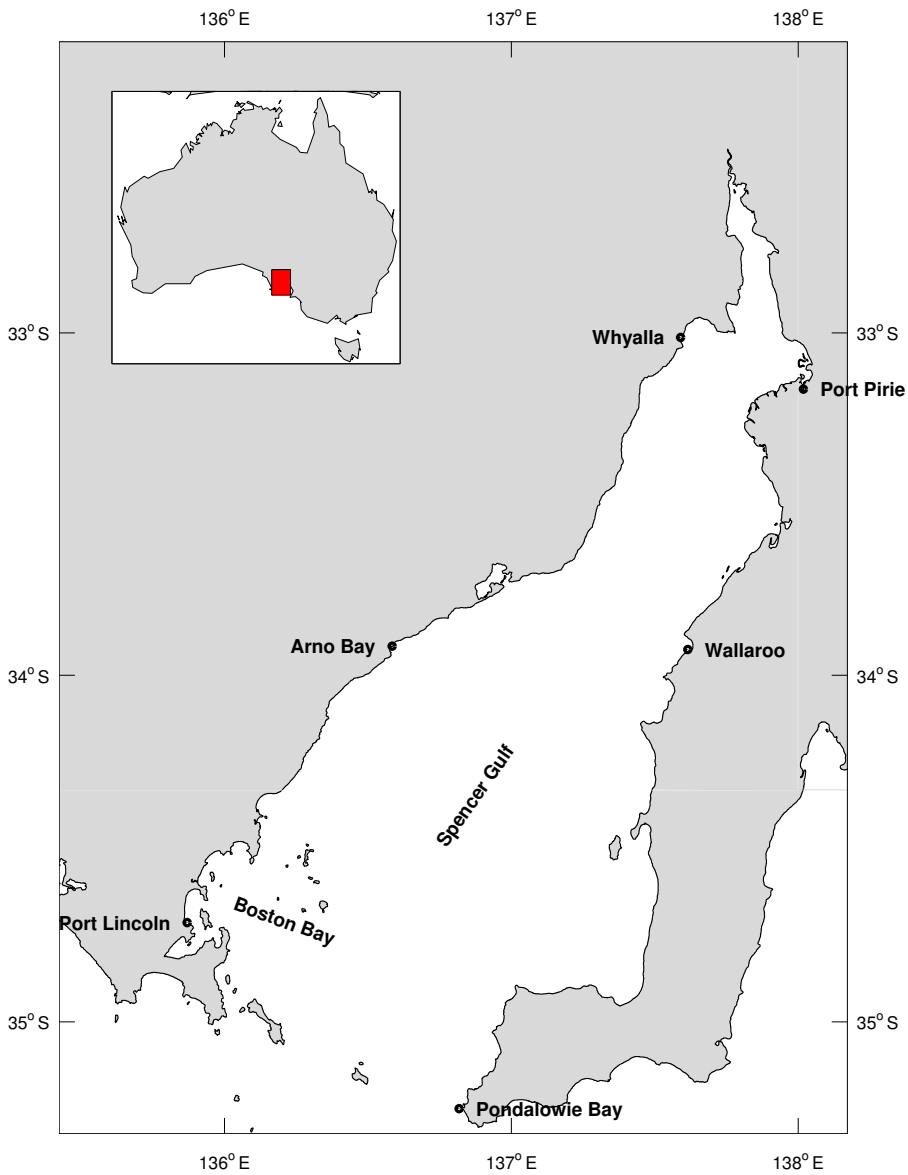

Figure 1.1. Spencer Gulf / Boston Bay region.

Studies of the tidal circulation of the gulf have been made (eg., Easton 1978; Nixon and Noye 1999) that show it to be a ¾ wave resonator, whereby the semi-diurnal constituents are amplified with current speeds of up to 50 cm s^{-1} mid-gulf. Additionally, because both the M2 and S2 tides have almost equal amplitude (but different frequency), these constituents interfere destructively leading to 4-5 day period every 14.8 days when the tidal velocities are small – the "dodge tide".

The gulf circulation driven by local meteorology and remote forcing is strongly seasonal. During winter, the westerly winds and atmospheric cooling combine to drive a westerly shelf circulation with water downwelled to depths of 300 m. Shelf current speeds of up to 1 m s^{-1} have been recorded on the shelf (Middleton and Bye 2007). Within the gulf, the atmospheric cooling is known to drive a clockwise circulation that appears to be modulated by the fortnightly dodge tide when the otherwise large (~50 cm s^{-1}) currents relax to near zero. Water is drawn in along the western side of the gulf and expelled past Kangaroo Island on the eastern side of the gulf.

During summer, evaporation is sufficient to make the gulf water denser than that found during winter, although significant gulf-shelf exchange is not observed. The reason for this appears related to the reversal of winds and resultant upwelling to the south-east of Kangaroo Island. Indeed, the analyses of Nunes Vaz et al (1990), Petrusivics (1993) and McClatchie et al (2006) suggest that the upwelled water forms a pool of sub-surface, nutrient rich water across the mouth of the gulf. This water is denser than that found in the gulf and may block its passage onto the shelf (Petrusivics 1993). Some penetration of upwelled water into the eastern side of the gulf is indicated from sea surface temperature data (see Middleton and Bye 2007). However, it may be possible that sub-surface intrusions do occur: little data has been collected to answer these questions.

The circulation driven by local winds and by the wind-driven circulation on the adjacent shelf has received little attention. Most recently, Middleton and Teixeira (2008) have shown that the gulf circulation driven by strong winds (10 m s^{-1}) is quite weak (< 5 cm s^{-1}) where the water depth is 10-20m or more. The reason for this is that the conditions of zero normal flow at coastal boundaries penetrate over a distance of the external deformation radius, that is, of order the width/length of the gulf. A similar result is found for the gulf circulation that is driven by (wind-driven) shelf circulation. As we will see from the study below, weak currents (< 5 cm s^{-1}) are found for the weather-band (3-20 days), both in the data and model. In shallow water (< 5m), the study of Middleton and Teixeira (2008) indicates that currents can be significantly larger (~15 cm s^{-1}) since the deformation radius is smaller.

During winter, the south-eastward winds expected to drive a clockwise circulation near the mouth of the gulf with water drawn in along the western side of the gulf and expelled along the Yorke Peninsula (Middleton and Teixeira 2008). This circulation should enhance that driven by dense water formation.

During summer, the winds and gulf circulation are expected to reverse, albeit with a weaker anticlockwise circulation near the gulf mouth (Middleton and Platov 2003; Middleton and Teixeira 2008). A schematic of the expected flow is shown in Figure 1.2. Consistent with this pattern, recent studies suggest that nutrient rich water should be drawn in along the eastern gulf mouth that arises from the summertime upwelling onto the shelf (Middleton and Teixeira 2008). As noted above, this water appears to prevent a strong gulf-shelf exchange that is found for winter (Lennon et al 1987).

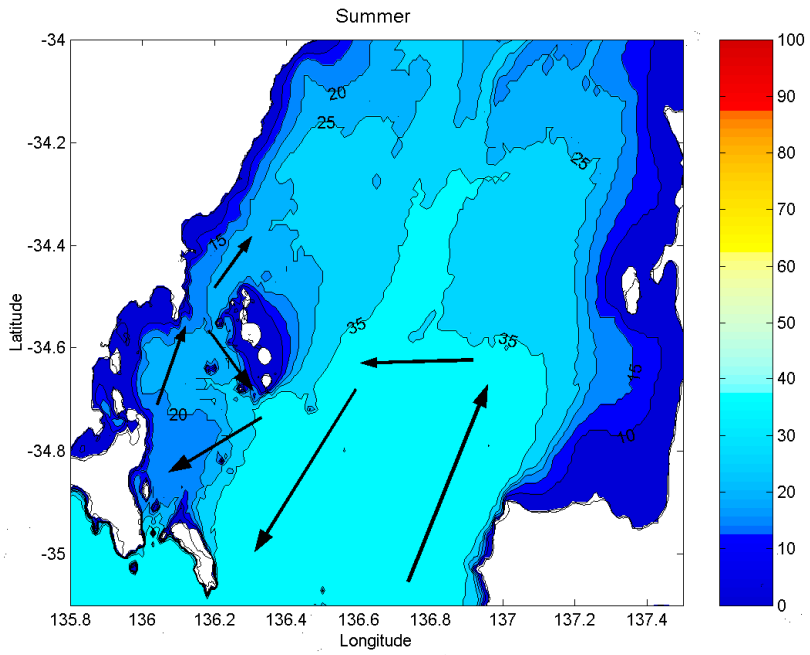

Figure1.2. The topography of the southern gulf region with the 0, 10, 15, 20, 25 35 m isobaths plotted. The arrows indicate expected flow due to mean summer winds. The arrow in the TFZ region corresponds to that estimated from the local model and data.

The numerical results will support the above conceptual model but with two additional complexities. The first is that when the waters are stratified, localized upwelling (downwelling) can occur for the Boston Bay region in the presence of eastward (westward) winds. Eastward winds drive surface gulf waters offshore that can drive a compensatory deeper onshore flow. On the adjacent shelf, eastward (westward) winds lead to downwelling (upwelling).

The second complexity arises from the topographic shielding of the TFZ from the larger gulf-scale summertime anticlockwise circulation. The local TFZ model and data below show that the flow past the region (along the 20 m depth contour) is to the north-north-east for all of the year. The larger gulf-scale regional model shows that the flow farther offshore (along the 30 m isobath) is to the south and south-west: this flow is essentially blocked by the Sir Joseph Banks group of islands that lie to the immediate north of the Boston Bay region.

While the wind-forced circulation (~ 5 cm s^{-1}) is smaller in magnitude than that of the 12 hourly tides (30-50 cm s^{-1}), we note here that the former persist for longer times (3 –20 days) and can be more important in terms of flushing of the region and in nutrient transport. Thus, both tidal and wind-driven motions are modelled in the study below, as are density currents that arise from atmospheric cooling and evaporation.

2. Objectives

In order to assess the physical characteristics of the TFZ, this study aims to implement a numerical hydrodynamic model that will provide predictive capacity for currents and mixing. The model is calibrated against data collected during field excursions. Insight into current regimes, flushing times, tracer dispersal distributions and residual flows can be gained from application of the model. The model is designed to aid in decisions regarding risks posed to the tuna industry, and assist in identifying mitigation strategies to those risks. The hydrodynamic model forms the basis for sediment transport and biogeochemical numerical investigations. The model was forced with atmospheric fluxes including wind stress, heat and freshwater exchanges, and with surface elevation, temperature and salinity on the offshore limits of the domain. A regional scale hydrodynamic model, which covers the whole of Spencer Gulf, is developed to establish boundary conditions for the local TFZ model. This model is represented with much larger resolution (~2-5 km) and covers a larger area, having the sole purpose of providing boundary conditions for the local model. The hydrodynamic model, its inputs, and model output, are discussed in more detail below. Analyses are presented addressing the flushing characteristics of the TFZ, passive tracer distributions in response to the circulation, residual flow dynamics and connectivity.

3. The Hydrodynamic Model

The hydrodynamic model used to simulate the flow and mixing of the TFZ is SHOC (Sparse Hydrodynamic Ocean Code; Herzfeld, 2006). This model has been developed by the Environmental Modelling group at CSIRO (Commonwealth Scientific and Industrial Research Organization) Division of Marine and Atmospheric Research over the last decade. SHOC is intended to be a general purpose model applicable to scales ranging from estuaries to regional ocean domains, and has been successfully applied to a variety of applications encompassing these scales to date. SHOC is a three-dimensional finite difference hydrodynamic model based on the primitive equations. Outputs from the model include three-dimensional distributions of velocity, temperature, salinity, density, passive tracers, mixing coefficients and sea level. The equations forming the basis of the model are similar to those described by Blumberg and Herring (1987). SHOC is based on the MECO model (Model for Estuaries and Coastal Oceans; Walker and Waring, 1998) with added functionality to allow distributed processing over multiple computing processors. SHOC also employs a sparse coordinate system internally that allows the representation of unused land in the model to be excluded. Inputs required by the model include forcing due to wind, atmospheric pressure gradients, surface heat and water fluxes, and open boundary conditions (e.g. tides). A schematic of the major forcing mechanisms captured by SHOC is included as Figure 3.1. SHOC is based on the three-dimensional equations of momentum, continuity and conservation of heat and salt, employing the hydrostatic and Boussinesq assumptions. The equations of motion are discretized on a finite-difference stencil corresponding to the Arakawa C grid.

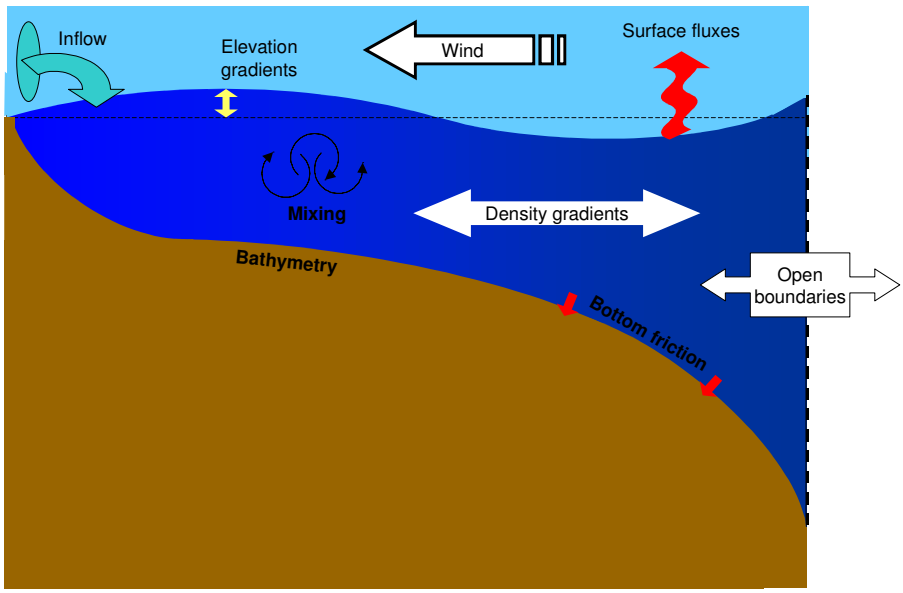

Figure 3.1. Schematic of forcing mechanisms in SHOC.

The model uses a curvilinear orthogonal grid in the horizontal and a choice of fixed 'z' coordinates or terrain following σ coordinates in the vertical. The curvilinear horizontal grid was particularly useful in this application since it enabled high resolution to be specified in areas of the study region where small-scale motions were present and larger resolution where

they were not. The ‘z’ vertical system allows for wetting and drying of surface cells, useful for modelling regions such as tidal flats where large areas are periodically dry. SHOC has a free surface and uses mode splitting (Simons, 1974) to separate the two-dimensional (2D) mode from the three-dimensional (3D) mode. This allows fast moving gravity waves to be solved independently from the slower moving internal waves, allowing the 2D and 3D modes to operate on different time-steps, resulting in a considerable improvement in computational efficiency. The model uses explicit time-stepping throughout except for the vertical diffusion scheme which is implicit. The implicit scheme guarantees unconditional stability in regions of high vertical resolution. A Laplacian diffusion scheme is employed in the horizontal on geopotential surfaces. Smagorinsky mixing coefficients may be utilized in the horizontal (Griffies and Hallberg, 2000).

SHOC can invoke several turbulence closure schemes, including k-ε, Mellor-Yamada 2.0 and Csanady type parameterisations. A variety of advection schemes may be used on tracers and 1st or 2nd order can be used for momentum. This study used the QUICKEST advection scheme for tracers (Leonard, 1979) in conjunction with the ULTIMATE limiter (Leonard, 1991). This scheme is characterized by very low numerical diffusion and dispersion, and yielded excellent performance when resolving frontal features, which often occurred during tracer analyses. SHOC also contains a suite of radiation, extrapolation, sponge and direct data forcing open boundary conditions. Input and output is handled through netCDF data formatted files, with the option of submitting ascii text files for simple time-series forcing. The netCDF format allows input of spatially and temporally varying forcing and initialization data in a grid and time-step independent manner. SHOC is capable of performing particle tracking and may be directly coupled to ecological and sediment transport models.

4. Model Domain

The simulation of the physics of the Boston Bay region required the construction of two model grids. The regional grid supplied the initial and open boundary conditions for a smaller local grid of the local study region, nested within the regional grid. In the absence of field-derived temperature, salinity and surface elevation measurements to apply to the open boundaries, this strategy is the only way of adequately driving the model through the open boundaries of the local model. The regional domain is illustrated in Figure 4.1 and the TFZ (local) domain in Figure 4.2.

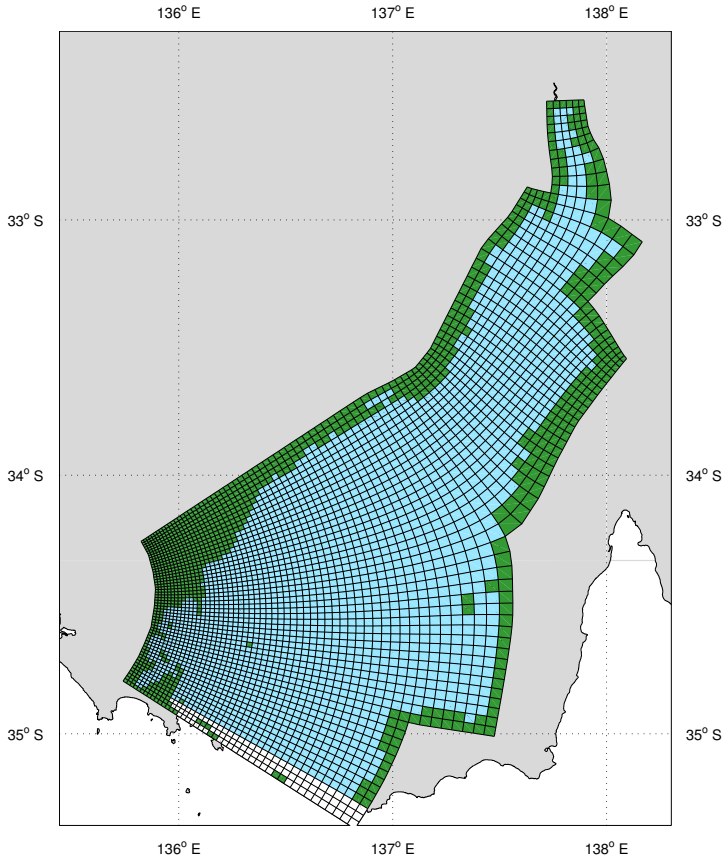

Figure 4.1. Regional Spencer Gulf domain.

The regional grid is curvilinear with variable resolution over the domain. Seaward of Boston Island the resolution is ~1500 m with resolution increasing to > 6 km on the eastern side of the gulf. The model uses 23 layers in the vertical with 0.5 m resolution at the surface and ~8 m resolution near the maximum depth of 60 m. The grid size is 55 x 95 x 23; 45% of surface cells are wet cells and 30% of all cells in the grid are wet. Run time ratios achieved were ~192:1 (i.e. the model simulates 192 days of results in 1 day of real time), allowing an annual simulation to be completed in ~2 days. The run-time ratio is determined by the stability constraints on the model, which limit the maximum time-step to be used for 2D and 3D modes, and are dependent on the grid resolution, the water depth, stratification and the size of the grid.

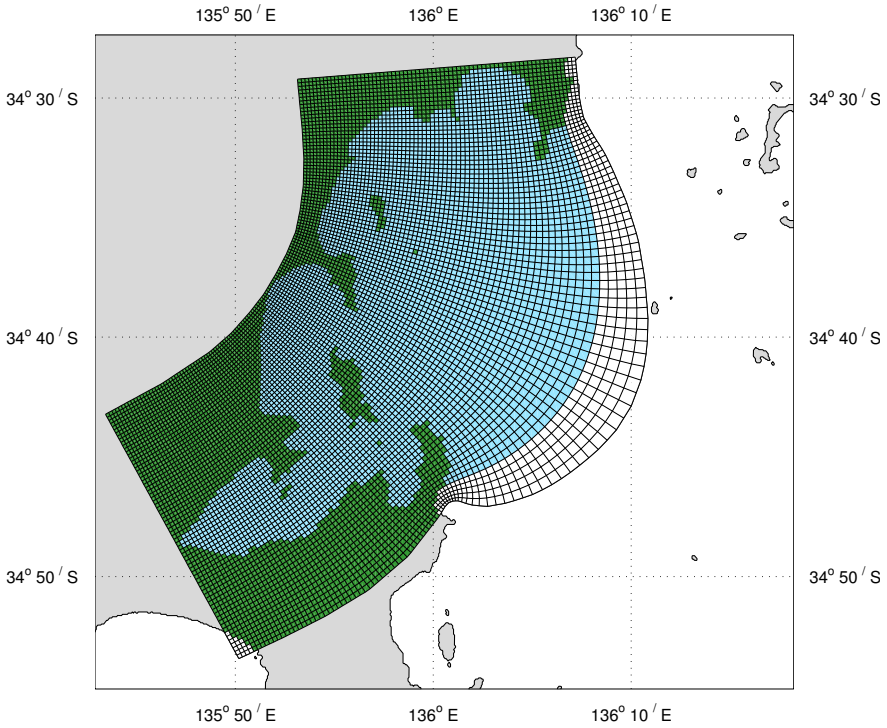

Figure 4.2. The tuna farming zone (TFZ) domain.

A curvilinear grid was also used to model the TFZ region. The grid spacing seaward from Boston Island is ~330 m and a maximum resolution of ~1 km exists on the offshore open boundary. The grid dimensions are 135 x 70 x18, with 0.5 m resolution in the vertical at the surface and ~4 m resolution at the bottom with a maximum depth of 30 m. This domain also consists of a high percentage of land cells, with 53% of the surface layer comprising wet cells and only 28% of the 3D domain being wet. Run time ratios achieved were ~90:1, allowing an annual simulation to be completed in ~4 days.

The seaward limit of the open boundary for the local model was based on the distribution of the tuna farming lease sites in 2005. It is acknowledged that these sites are subject to change, and there is a tendency for leases to be granted further into Spencer Gulf. Obviously the modelling cannot anticipate future lease configurations, hence it was considered appropriate to define the offshore limit of the local model based on the lease configuration of mid-2005 (Figure 4.3). As information became available, it was evident that leases were in fact edging into deeper water, and some of the proposed leases for 2006 were impinging on the local grid open boundary (Figure 4.4). The model domain was defined on the basis of information available at the commencement of the project, which encompassed all lease sites positioned during 2005.

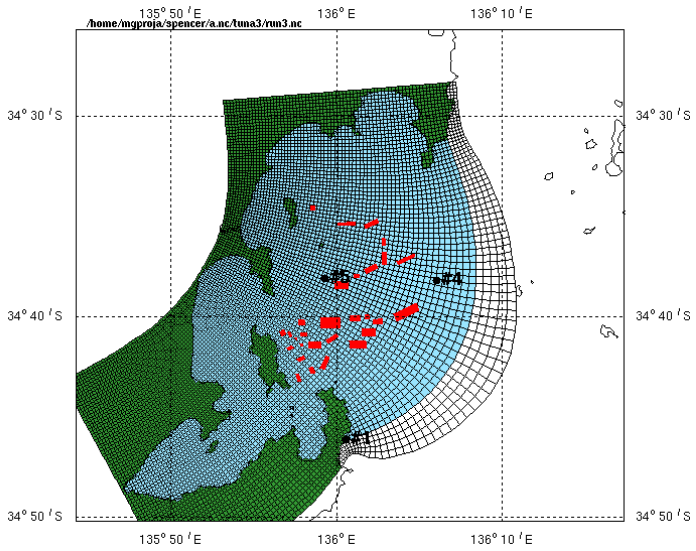

Figure 4.3. Lease sites at commencement of the study; 2005.

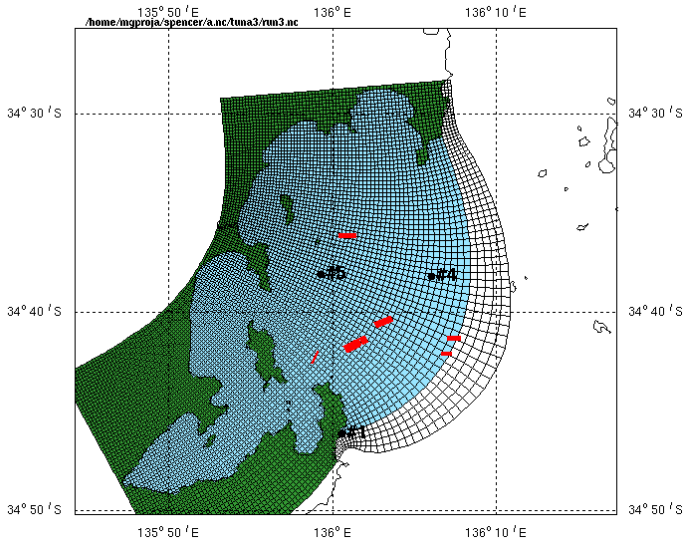

Figure 4.4. Differences in proposed 2006 lease sites.

5. Input Data

The model was forced with surface atmospheric fluxes (wind, heat and freshwater), and elevation, temperature and salinity on the open boundaries. A field program was implemented to supply data to force the open boundary of the regional model, and to supply calibration data for both models. The simulation period, defined by availability of data from this field program, was chosen as 2 Sep 2005 to 11 Aug 2006 inclusive, providing ~12 months of simulation. The sources of the forcing data are detailed below.

5.1. Bathymetry

The bathymetry for the regional model was interpolated from Geoscience Australia's 1 km bathymetric product (Petkovic and Buchanan, 2002). The bathymetry for the TFZ region was initially interpolated from Geoscience Australia's 2005 product at 250 m resolution, but as this inadequately represented the bathymetry of the region, it was supplemented with digitized bathymetry from the AUS134 navigational chart. The final bathymetry used for the TFZ is displayed in Figure 5.1.1. Overlaid on this figure are the 2005 lease site locations, and the locations of the moorings deployed in the TFZ (see Section 6).

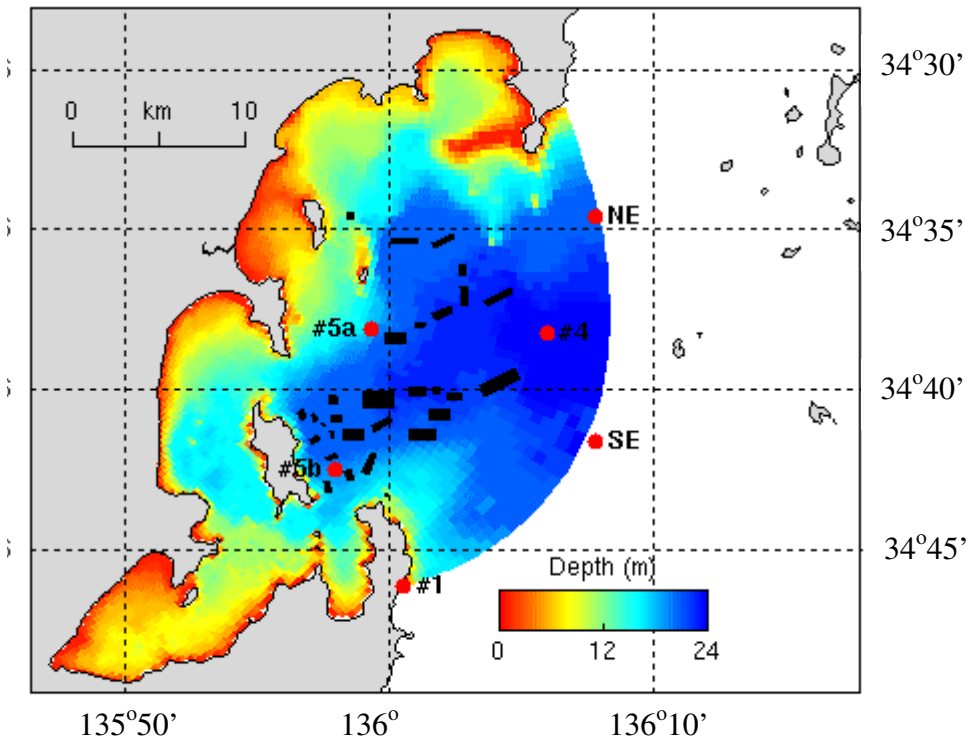

Figure 5.1.1. Bathymetry of the tuna farming zone region. NE and SE refer to the limits of the tuna farming zone designated during 2005. Numbers indicate mooring locations (see Section 6.1).

5.2. Wind Forcing

Wind speed and direction data were obtained from the Bureau of Meteorology at the locations depicted in Figure 5.2.1 and interpolated onto the regional domain to provide a temporally and spatially varying wind-field.

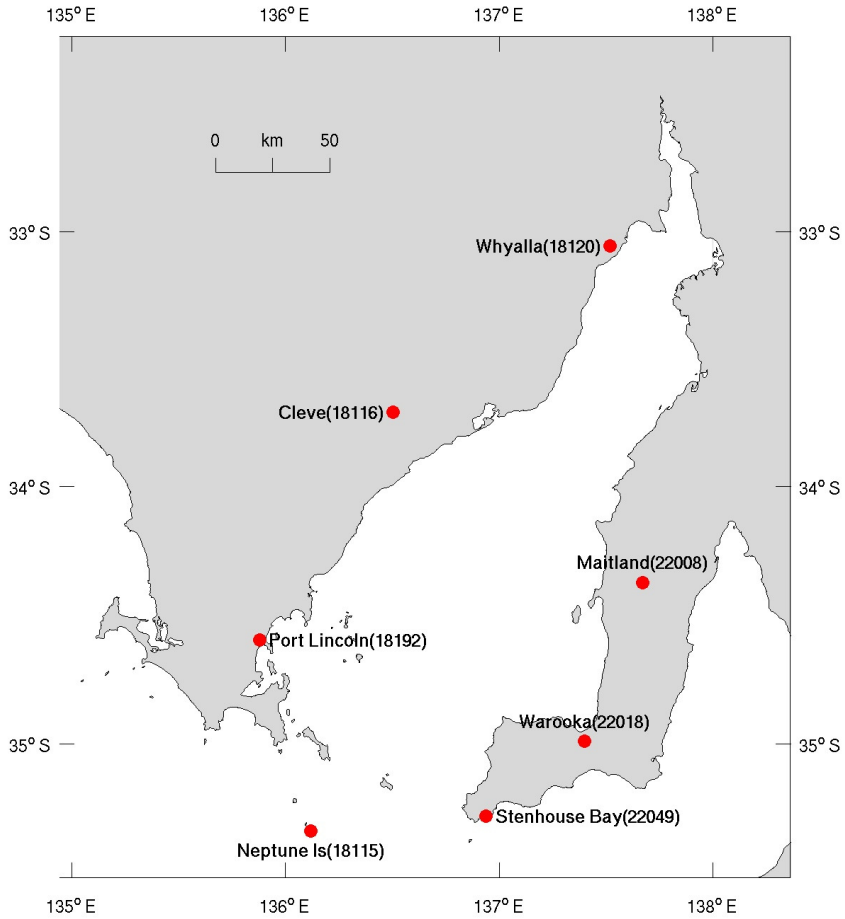

Figure 5.2.1. Wind Measurement sites. Numbers in brackets indicate the number of measurements taken during the simulation period.

A sample of the wind-field at selected sites is shown in Figure 5.2 for the simulation period. The mean wind speed and direction during the whole period is shown in Table 5.1.

Table 5.1. Mean wind speed and direction for wind measurement sites

Site	Annual Mean Wind Speed ($m\ s^{-1}$)	Annual Mean Wind Direction (°T)
Cleve	5.3	192
Port Lincoln	5.1	208
Neptune Island	8.2	178
Stenhouse Bay	6.1	192
Warooka	3.2	202
Maitland	2.9	192
Whyalla	4.8	211

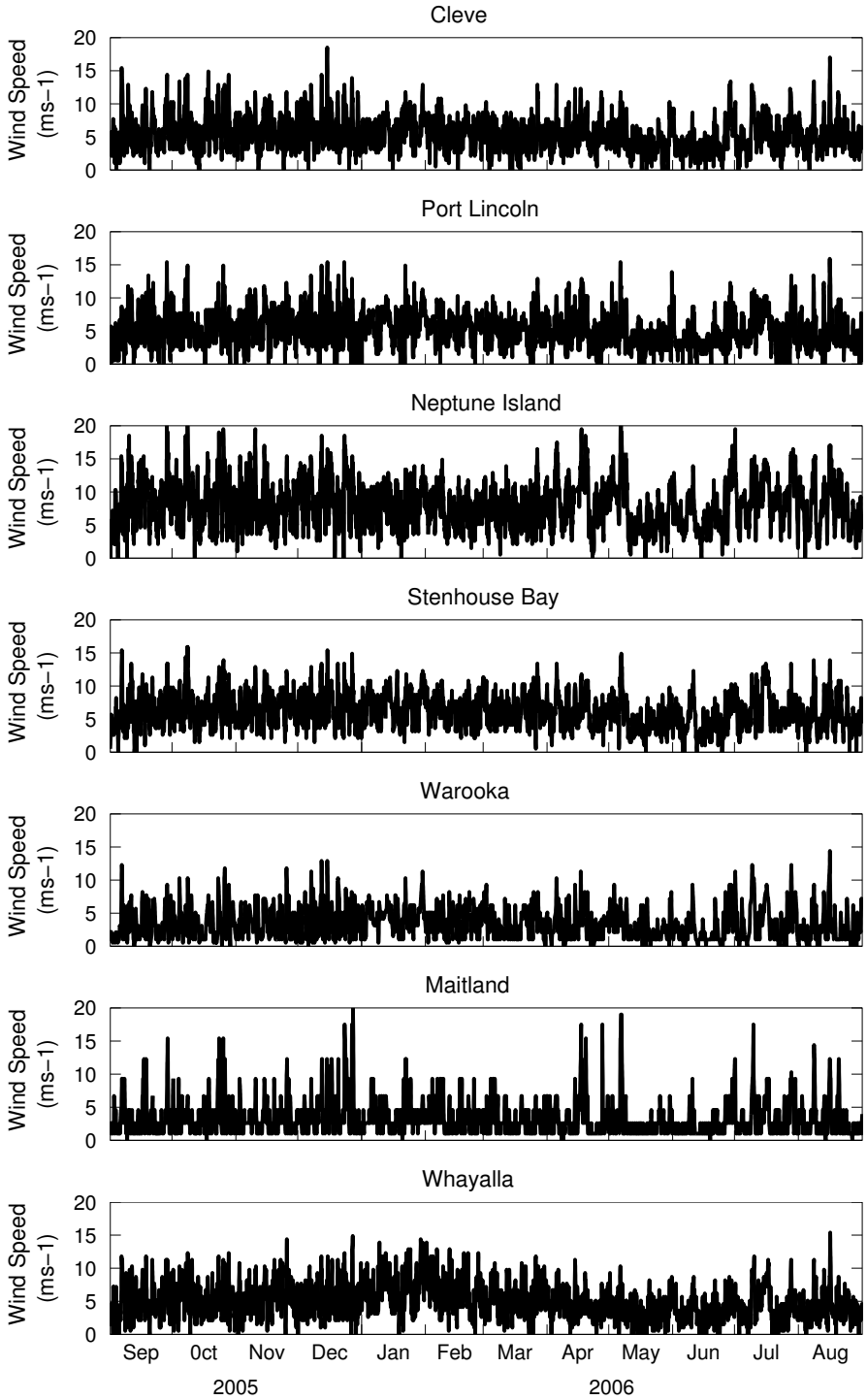

Figure 5.2.1. Wind speed at measurement sites.

Figure 5.2.1 and Table 5.1 indicate that for the simulation period, the mean wind in the TFZ region was a relatively light (~5 m s^{-1}) southerly. Wind speed is generally below 15 m s^{-1}, with the southern most sites and those on the western side of the gulf experiencing higher wind-speed.

5.3. Surface Elevation

The time series of surface elevation prescribed on the open boundaries of the local TFZ model were supplied from output of the regional model. The elevations used in the regional model consist of a high frequency component (tidal component with periods < 1 day) and a low frequency component with periods of days to weeks. Measurement sites for which sea level data were obtained are illustrated in Figure 5.3.1.

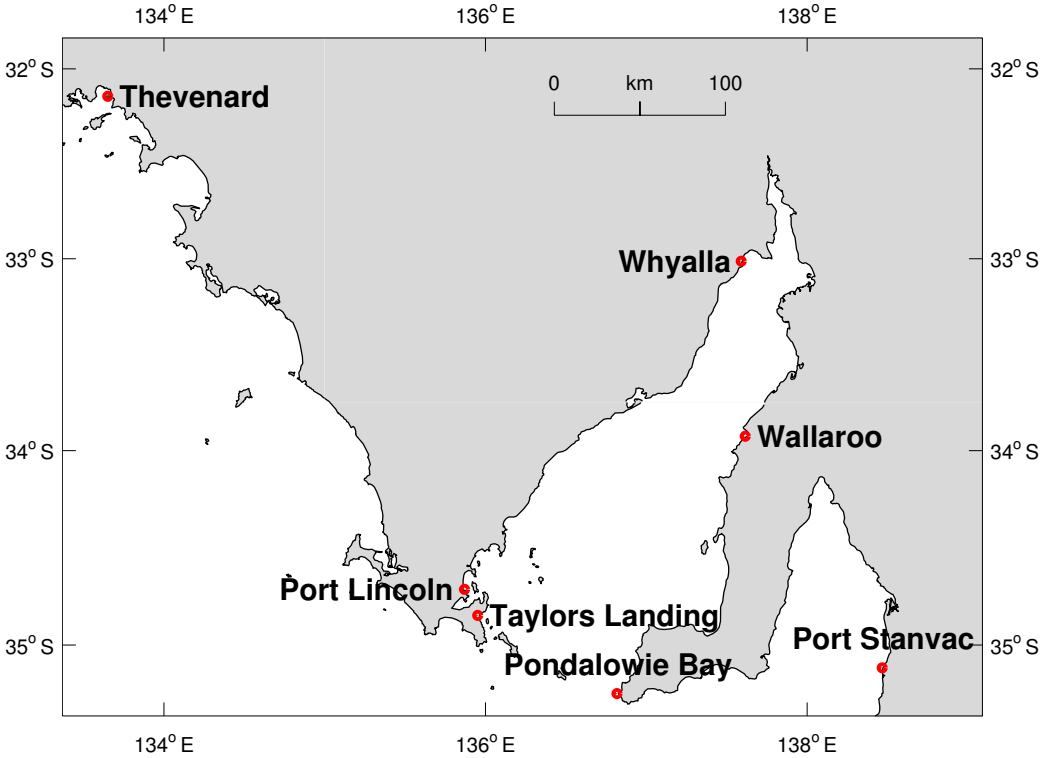

Figure 5.3.1. Tidal measurement locations.

There are two components of forcing needed at the mouth of the gulf for the (large scale) regional model. We first discuss forcing in the tidal band and then forcing in the weather band (typically 3 days or longer).

Tidal-band Forcing

The open boundary of the regional model fortuitously corresponded to a linear transect between Taylor's Landing and Pondalowie Bay, and to a lesser extent Thevenard and Port Stanvac. This allowed the tidal harmonics and low frequency signal corresponding to these measurement sites to be linearly interpolated along the open boundary of the regional model. The tidal harmonics for Taylor's Landing and Pondalowie Bay (obtained from http://www.flaterco.com/xtide/) allowed the phase and amplitude of the 14 largest constituents (see Table 5.3.1) to be linearly interpolated along the open boundary of the regional model. The tide was then reconstructed from this information at the open boundary nodes to create the tidal sea level response along the regional domain seaward boundary.

Table 5.3.1. Tidal harmonics for Taylor's Landing

Constituent	Amplitude (m)	Phase (Deg)
M2	0.2013	17.75
S2	0.2109	67.80
K1	0.2105	24.49
O1	0.1528	358.26
S1	0.0075	139.10
Q1	0.0329	336.19
P1	0.0679	18.01
N2	0.0159	97.48
NU2	0.0	0.0
K2	0.0615	69.18
L2	0.0146	57.62
2N2	0.0100	83.31
MU2	0.0120	98.60
T2	0.0167	73.41

It is observed from Table 5.3.1 that the dominant constituents in the region are those due to M2, S2 and K1, all of which have approximately the same amplitude. It is the similarity between the amplitude of the semi-diurnal components that allows the unique phenomena of the dodge tide to occur in Spencer Gulf; this occurs when M2 and S2 are exactly out of phase, therefore cancelling and resulting in no tidal movement (and hence no currents) for the tidal period.

Weather-band Forcing

Sea level signals across the gulf mouth need to be prescribed that correspond to forcing by local winds and the wind-forced shelf circulation. Unfortunately, the sea level records from M1 and M2 were found to have datum shifts of 10 – 20 cm brought about by re-deployment of the instruments at slightly different depths after servicing (Table 6.1 below). Such datum shifts must be eliminated if the data is to be used to drive the model open boundary for periods longer than the minimum period of co-incident data (42 days). In addition, due to lack of equipment, the pressure sensors adopted for moorings M1 and M2 only give approximate depths with an accuracy of a centimetre or so. Moreover, no averaging was made to eliminate aliasing due to waves: sea level heights were recorded instantaneously every 15 minutes. Mooring M3 did use a high quality tide gauge sensor and every 15 minutes samples were obtained as burst (4 minute) averages. Thus, the quality of the M1 and M2 sea level data remains to be determined.

To this end a re-analysis is made (Appendix A) of the low-passed filtered sea level data from the gulf sites M1 to M5. First, the low-pass filtered data at site M5 is found to be very similar to that at site M1 so that data from the former (M5) can be used to produce a long 10 month time series of continuous data at site M1.This also gives confidence in the M1 data collected. Similar continuous data sets are obtained for site M2 and M3. The mean seasonal sea level signal at M3 (~ 10 cm) is assumed for sites M1 and M2 and the underlying assumption is that no net geostrophic flow into the gulf occurs for periods of two months or greater.

The use of these (uncertain) time series is discussed in section 7.3. As an alternative, continuous time series of sea level were also obtained for Thevenard and Port Stanvac from the National Tidal Centre (NTC) and used to extract the low frequency signal. This signal propagates anti-clockwise around the Australian coast, and a lag of 7.68 hours was computed between Thevenard and Port Stanvac. The lag between any open boundary node and

Thevenard could then be computed as a fraction of this lag. The amplitude of the low frequency signal at each open boundary node was calculated using a weighted interpolation in time and space between the Thevenard and Port Stanvac data, and applied at the correctly lagged time relative to Thevenard. The sea level was then linearly interpolated across the gulf mouth. The seaward boundary in the model was forced with the tidal and weather-band sea levels using relaxation to a gravity wave radiation condition with a time-scale of 30 minutes following the methodology of Blumberg and Kantha (1985).

5.4. Temperature and Salinity

The initial conditions for temperature and salinity for both regional and local grids were derived from the product synTS (Ridgway et al., 2006). This product uses satellite altimetry to prescribe surface temperature and sea level distributions, then utilizes correlations based on climatology to project the surface distributions through depth. Resolution is 0.25 degrees. The initial temperature and salinity distributions over the regional domain are illustrated in Figure 5.4.1.

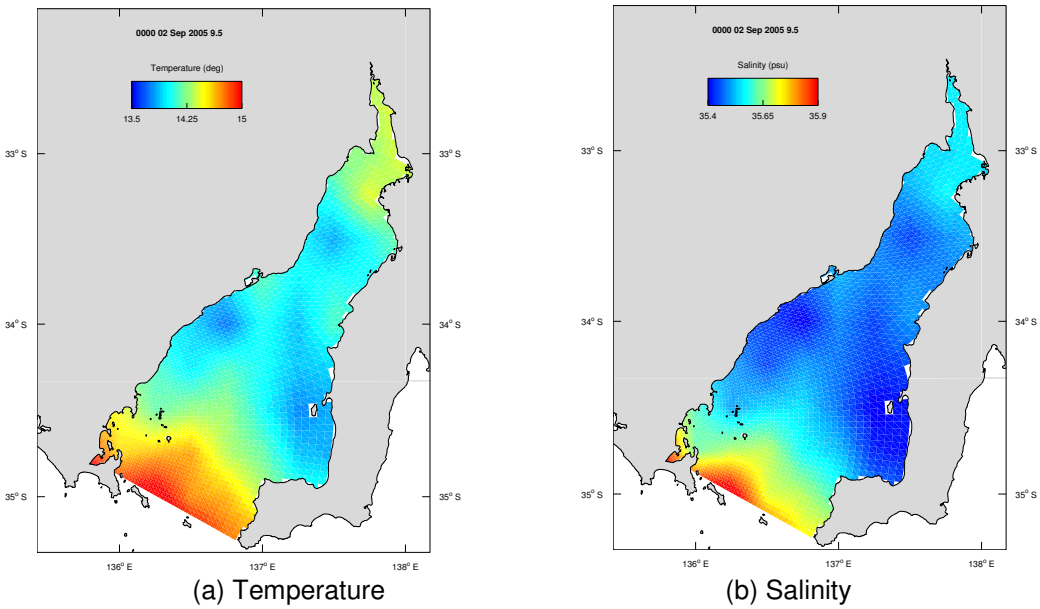

Figure 5.4.1. Initial conditions for the regional grid derived from synTS.

The open boundary forcing for the regional model was derived from measurements obtained from the moored instruments across the mouth of Spencer Gulf (see Section 6). These instruments provided temperature and salinity at the surface on the eastern and western sides of the gulf, and at the deepest location mid-gulf. These surface and bottom data were used as endpoints of a profile of temperature and salinity (T/S); the depth distribution of T/S between these endpoints was scaled to a time dependent density profile obtained from the model during its simulation at a location 10 grid cells into the interior of the domain from the open boundary.

5.5. Heat and Salt Fluxes

Heat fluxes were computed from standard meteorological measurements by the methods outlined in Herzfeld (2005, Chapter 9). Short wave radiation was estimated from the sun's hour angle at the latitude corresponding to Spencer Gulf, and corrected for (measured) cloud cover. Long wave radiation was calculated using the model sea surface temperature and

measured air temperature, also correcting for cloud. Sensible and latent heat fluxes were calculated using the bulk method of Kitaigorodskii et al. (1973), which required wet and dry bulb air temperature, pressure and wind-speed measurements as input. The heat flux components for the simulation period were computed from atmospheric data collected at Warooka, and are illustrated in Figure 5.5.1.

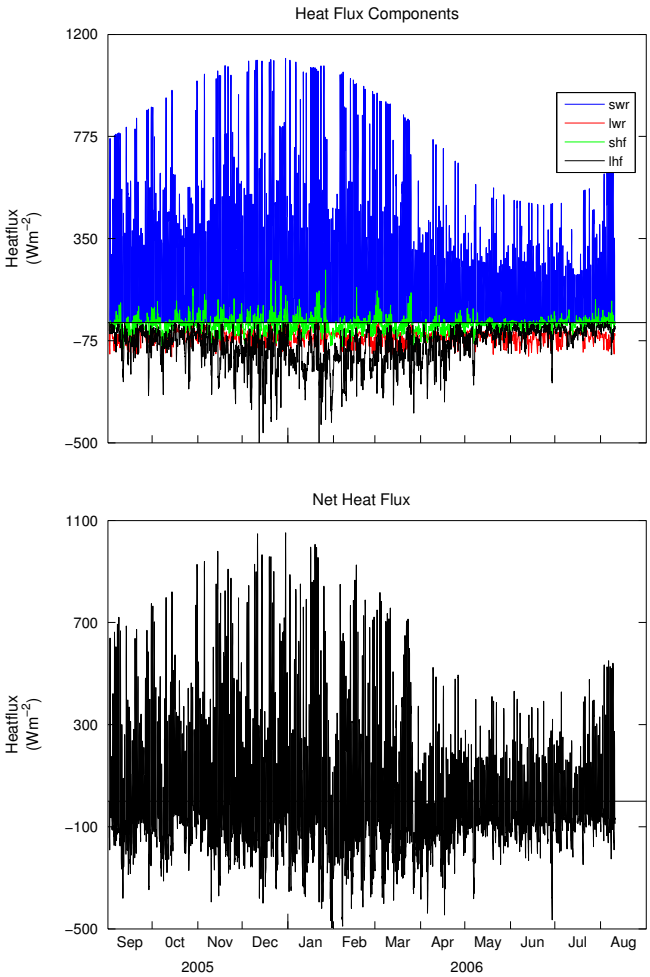

Figure 5.5.1. Heat fluxes calculated for Spencer Gulf based on atmospheric data obtained from Warooka. Swr – short wave radiation, lwr – long wave radiation, shf – sensible heat flux, lhf – latent heat flux.

The salt flux is defined as the difference between evaporation and precipitation. Rainfall was spatially and temporally interpolated from the meteorological sites illustrated in Figure 5.2.1. Evaporation over water is difficult to measure, and was estimated from monthly means provided by the bureau of meteorology (http://www.bom.gov.au/cgi-bin/climate/cgi_bin_scripts/evaporation.cgi) at locations corresponding to Port Augusta and Yorketown at the end of Yorke Peninsula. Differences in air – sea temperature can initiate a stable layer above the sea surface which suppresses evaporation, resulting in differing evaporation rates over the ocean compared to those over land. This typically requires the application of a pan factor to land based evaporation measurements to provide rates applicable over the ocean. These pan factors are the ratio of the evaporation rate over the ocean to that encountered over a standard meteorological evaporation pan under similar atmospheric conditions. Pan factors are usually < 1.0, and were treated as calibratable parameters in this study, varying linearly from the southern boundary

to the head of the gulf. Evaporation rates used in regional and local grids in the TFZ and the head of the gulf are displayed in Figure 5.5.2.

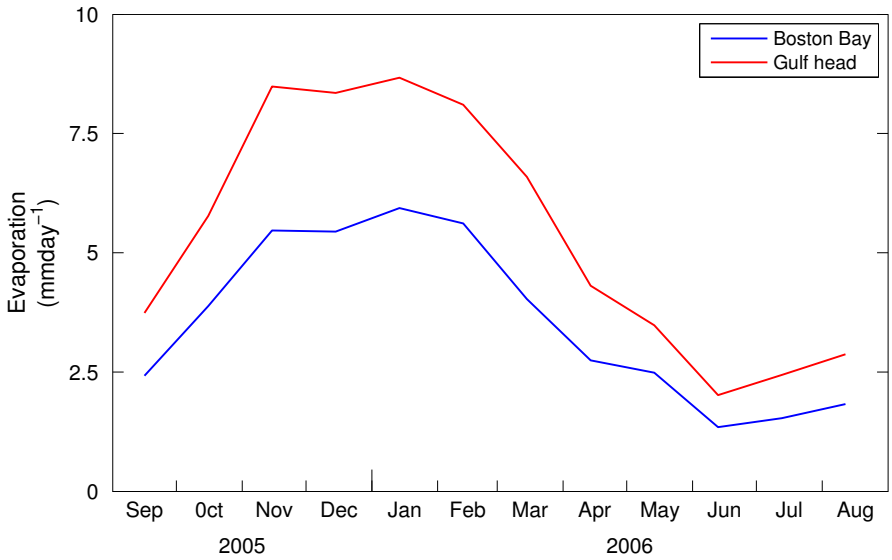

Figure 5.5.2. Estimated evaporation rates in Spencer Gulf.

6. Measured Data

6.1. Fixed Moorings – an overview

Between August 30 2005 and September 1 2006, a series of oceanographic moorings were placed across the mouth of Spencer Gulf and in and around the tuna-farming zone (Figures 6.1.1 and 6.1.2). Shallow moorings (3-5 m) were placed on either side of the mouth at Pondalowie Bay (mooring 2) and Carcasse Rock (mooring 1. e.g. Figure 6.1.3) to measure conductivity, temperature and depth, while a similar deep-water mooring (50 m), also incorporating a tide gauge, was placed in the middle of the mouth of the gulf, north of Wedge Island (mooring 3). The two moorings in the farming zone measured conductivity, temperature, depth, light and chlorophyll levels, and were also configured with ADCPs to measure current speeds throughout the water column (e.g. Figure 6.1.4, mooring 4). All shallow water moorings were successfully serviced on a three monthly basis, when data was downloaded, moorings cleaned and then redeployed. Fouling was an issue on many of the moorings (Figure 6.1.5), and may have compromised data quality on occasion. Mooring 5 was relocated to new positions in the TFZ on these servicing events. Due to its location, mooring 3 required a reasonable sized vessel to perform the deployment, hence was only serviced once (in February). During the May 2006 service, mooring 5 was re-located south of its previous position (from 5c to 5d), mooring 4 was re-located to lie further north-east on the model open boundary (from 4c to 4d) and an extra mooring was deployed (mooring 6) having the same configuration as mooring 4 minus an ADCP. These moorings collected data that is essential for developing the proposed hydrodynamic models, as well as data for calibrating the biogeochemical model. The locations and turn-around details are displayed in Table 6.1.

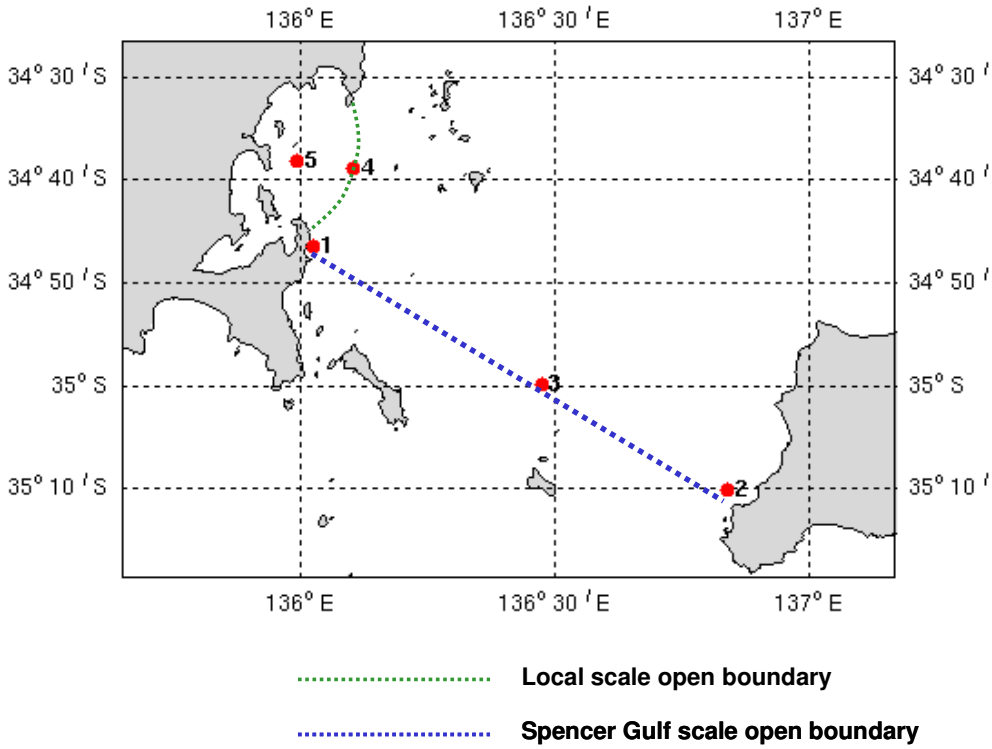

Figure 6.1.1. Location of moorings deployed in Spencer Gulf. The local scale open boundary indicates the extent of the detailed model, which is influenced by what happens in the less detailed model of Spencer Gulf.

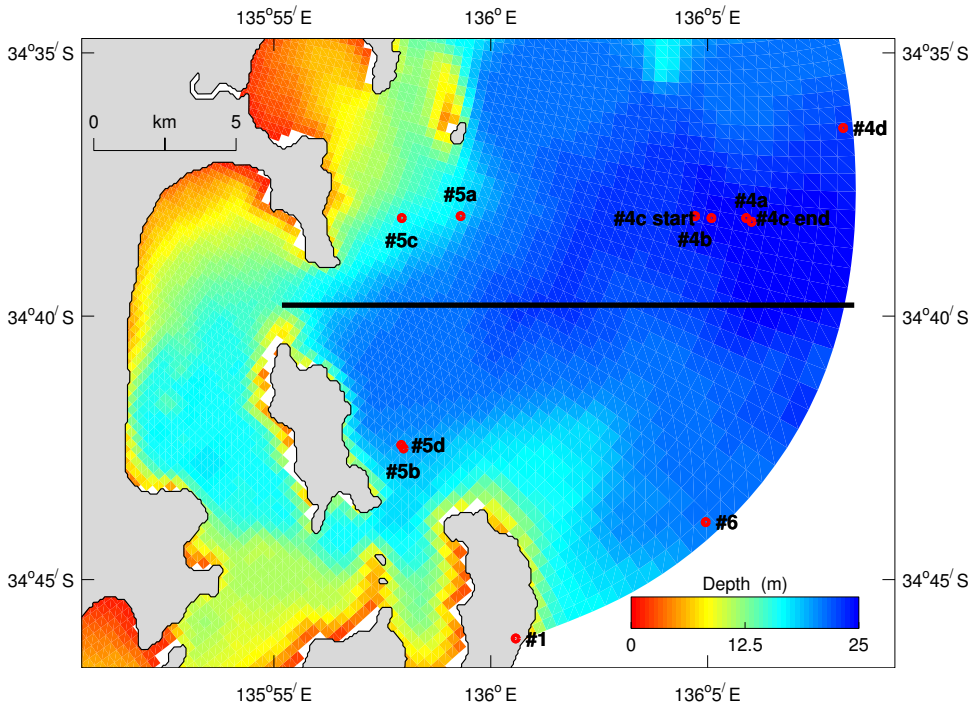

Figure 6.1.2. Details of moorings deployed in the TFZ. Mooring 4 was dragged during deployment #3; start and end locations are denoted 4c_start and 4c_end respectively. The thick black line corresponds to a CTD transect that was sampled monthly (see below).

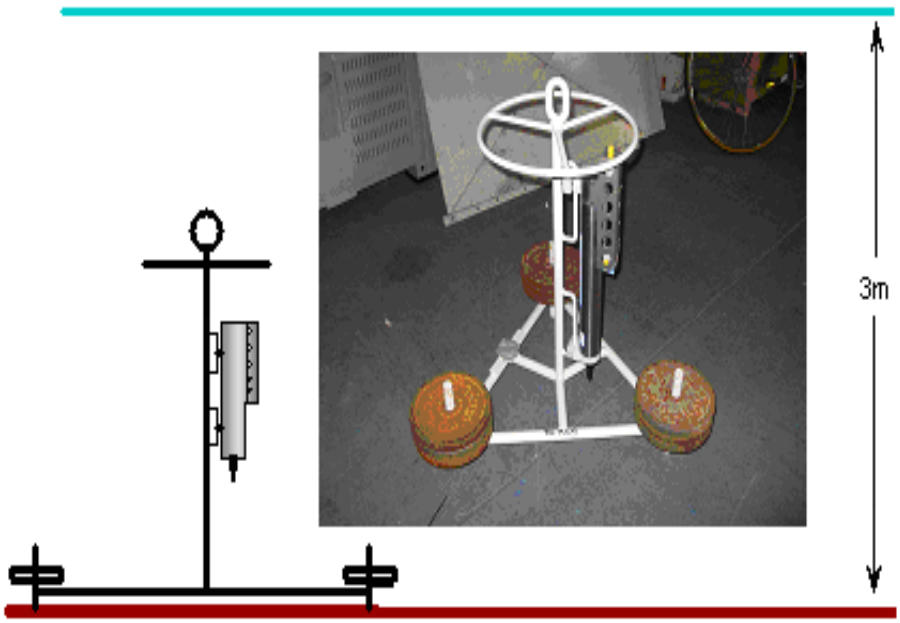

Figure 6.1.3. Mooring 1 & 2 configuration.

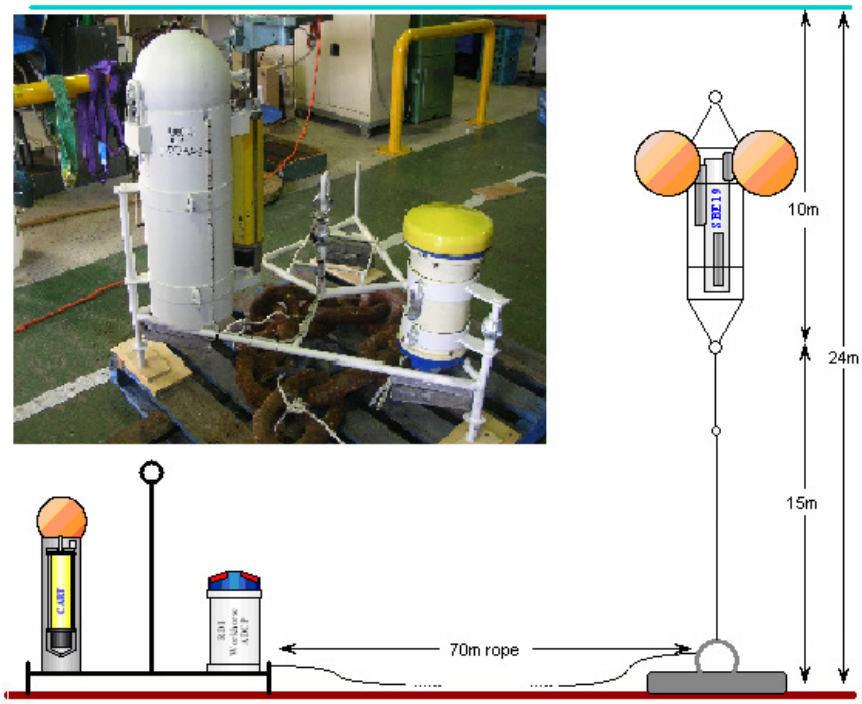

Figure 6.1.4. Mooring 4 configuration.

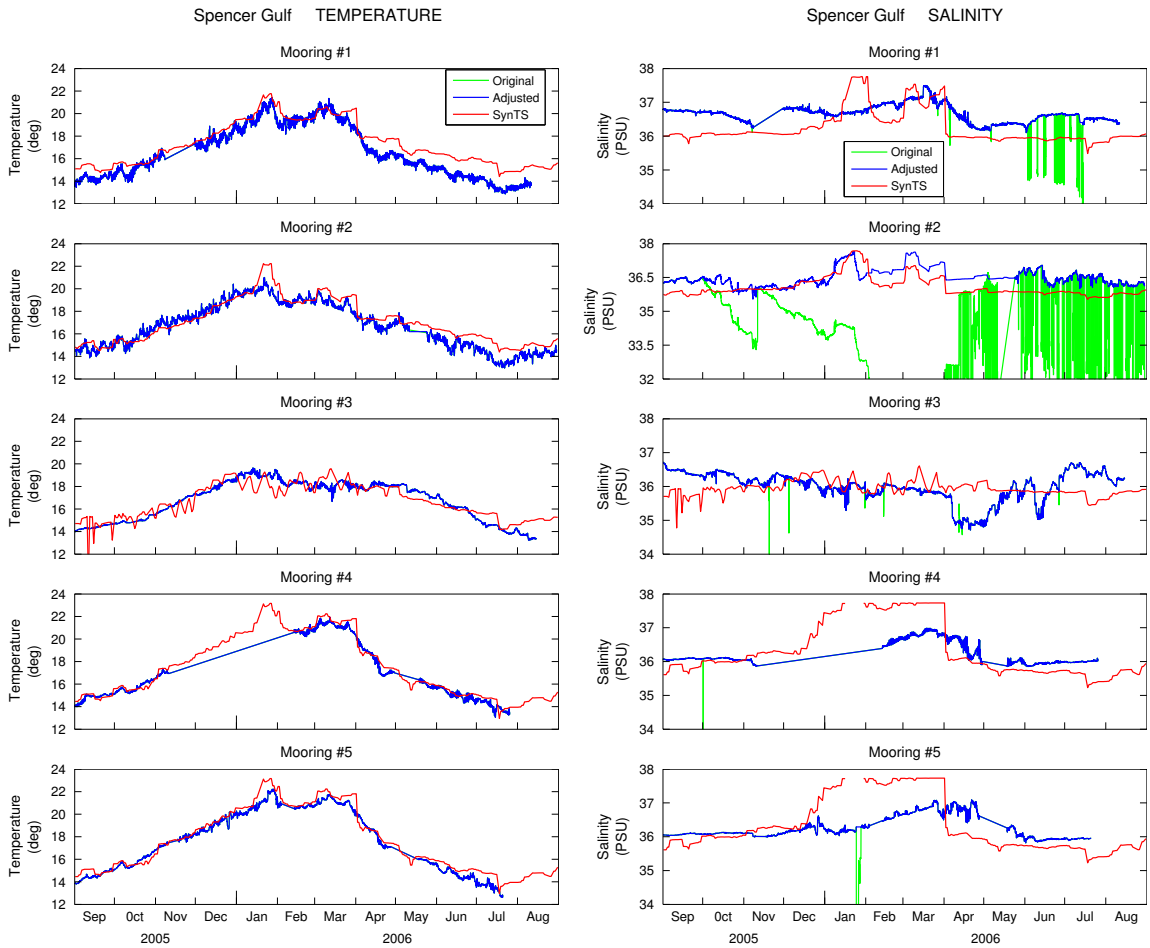

Figure 6.1.5. Raw and processed temperature and salinity time series.

Table 6.1. Mooring location and deployment details.

Mooring 1

Deployment	Date (local)	Sensor Depth (m)	Latitude	Longitude
Seabird Microcat with depth sensor				
1	31/0805 08:55	4.4	34 46.118S	136 00.576E
2	30/11/05 8:50	4.8	34 46.118S	136 00.576E
3	16/03/06	4.3	34 46.118S	136 00.576E
4	18/5/2006 17:40	4.8	34 46.108S	136 00.600E

Mooring 2

Deployment	Date (local)	Sensor Depth (m)	Latitude	Longitude
Seabird Microcat with depth sensor				
1	1/9/05 12:41	~5	35 13.873S	136 50.371E
2	11/11/05 10:10	~5	35 13.873S	136 50.371E
3	01/02/06	5.38	35 13.873S	136 50.371E
4	24/05/06 13:10	5.40	35 13.873S	136 50.371E

Mooring 3

Deployment	Date (local)	Sensor Depth (m)	Latitude	Longitude
Seabird Microcat with depth sensor + Seabird SBE 26 Integrating tide gauge				
1	1/9/05 09:15	48.33	35 00.089S	136 27.968E
2				
3	14-Feb-06 17:15	48.47	35 00.086S	36 27 .989E
4				

Mooring 4

Deployment	Date (local)	Sensor/Water Depth (m)	Latitude	Longitude
Seabird * SBE19 + RDI Workhorse 600Khz (High resolution model)				
1	31/08/05 11:23	13.80/24	34 38.206S	136 06.011E
2	17/11/05 11:40	?/22	34 38.101 S	136 04.711 E
3	13/Feb/06 10:20	9.66/22	34 38.137 S	136 05.090 E
4	18/5/2006 13:20	9.04/22	34 36.425S	136 08.126E

Mooring 5

Deployment	Date (local)	Water Depth (m)	Latitude	Longitude
Seabird * SBE19 + Nortek Aquapro 1Mhz Adcp (with external battery pack)				
1	31/0805 10:20	18.53/20	34 38.099S	135 59.306E
2	17/11/05 10:25	19.89/18	34 42.508 S	135 57.993 E
3	13/Feb/06 11:31	20.05/18	34 42.465 S	135 57.946 E
4	18/5/2006 11:30	20.13/18	34 42.446S	135 57.938E

Mooring 6

Deployment	Date (local)	Water Depth (m)	Latitude	Longitude
Seabird * SBE19				
1	18/5/2006 15:05	~20	34 43.908S	136 04.953E

6.2. Temperature/Salinity Mooring Data

Overall, the quality of data retrieved from the moorings is fair. Temperature and salinity are displayed in Figure 6.1.5. Mooring #4 lost all data for the second deployment; temperature appears reasonable for all other deployments. Salinity suffers from several obvious problems. Mooring 1 is ~0.7 psu saltier than mooring 4 and 5, although the lateral distance between all three moorings is not great. It is considered unlikely that such a large salinity gradient could exist in the absence of reasonable freshwater or salt input fluxes. Mooring 2 becomes fresher throughout the course of the first and second deployments. After the first turnaround salinity jumps markedly, indicative of a systematic drift of the salinity sensor. The third deployment produced no reasonable salinity data for mooring 2, and data from synTS was substituted for this period with a 0.6 psu offset applied. The fourth deployment contained an excessive number of spikes. Mooring 3 looks reasonable except for the odd low salinity spike. As mentioned above, mooring 4 lost all data for the second deployment, otherwise data looks reasonable. Mooring 5 has an anomalous spike in the data toward the end of January, otherwise also looks reasonable.

These errors in the salinity measurements can be managed to a certain extent by interpolating over gaps and de-trending salinity drifts. The adjusted salinity to be used as model input is also displayed in Figure 6.1.5. The synTS T/S is included in Figure 6.1.5 for reference. Note that synTS is the most accurate derived product suitable for analysis of temperature or salinity available.

6.3. Transect and SST Data

To put the above time series in context, we next discuss the SST and transect data obtained for the region. The transect data was obtained monthly (from September 2005 to August 2006) and along a zonal path, just south of M4 and M5- see Figure 6.1.2. Only valid data that largely covered the section is discussed. We begin with the SST image (MODIS) shown in Figure 6.3.1 for November 2nd 2005.

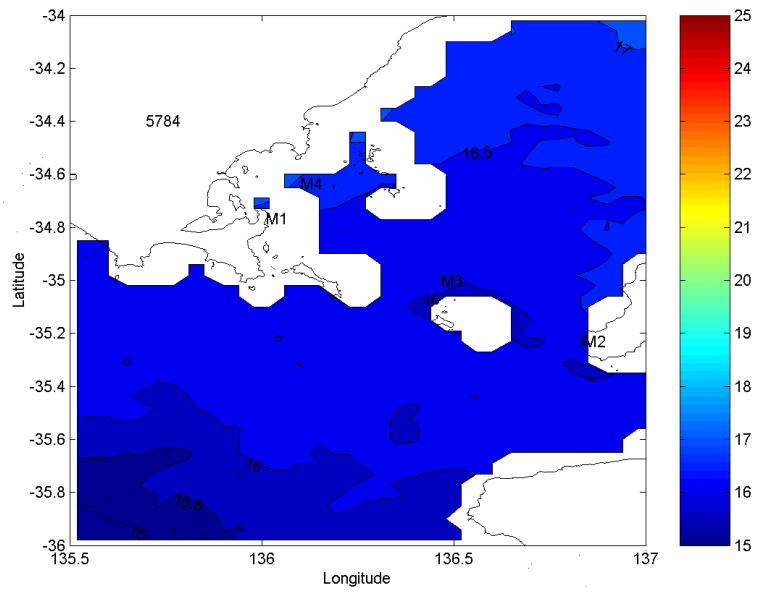

Figure 6.3.1. MODIS SST for November 2nd 2005 (JD 5785). Contour interval is 0.5 ˚C.

As is evident, there is little spatial variation and the cool 16 °C water is indicative of winter conditions. Indeed, the wind stress to this time (JD 5785), and up until the end of 2005 (JD 5842), is characterized by a mean direction to the east and by the passage of strong storms (0.1-0.2 Pa) every 3-20 days (Figure 6.3.2).

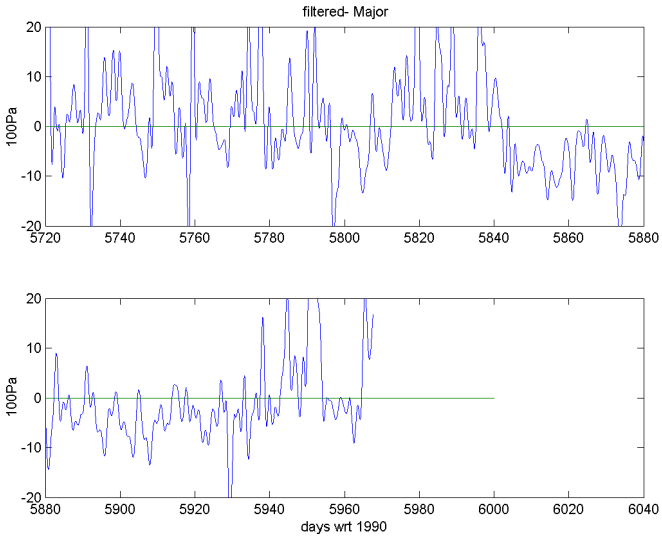

Figure 6.3.2. Major component of wind stress (Thompson Filtered; Units 100Pa). The major component was resolved to be that along the shelf and is positive to the S.E.

After November, the gulf waters warm (Figure 6.1.5) due to solar heating. In Figure 6.3.3, we present the temperature from M5 along with a synthetic time series based on the net daily heat flux for the region and an assumed depth of 20 m (see Appendix B). The synthetic time series is based on the daily temperature changes so determined and an assumed initial temperature from the M5 mooring: taken on December 6th 2005 (JD 5818).

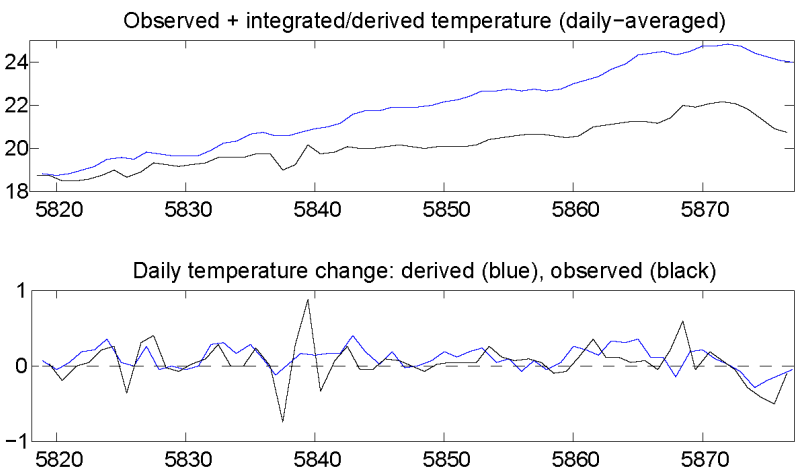

Figure 6.3.3. Upper panel: observed temperature at Mooring 5 in the TFZ (black line) and predicted temperature based on modelled heat flux assuming the same starting temperature (blue line). Bottom panel: Daily changes in temperature for the observed and predicted time series. The start and end dates (days 5818 and 5877) are 6 December 2005 and 3 February 2006.

As is evident, part of the daily temperature changes can be explained by local solar heating. The general increase in temperature is also captured, although the simple model leads to higher temperature than observed.

By December 28th, 2005 (JD 5840), the winds reverse to become upwelling favourable for the shelf (Figure 6.3.2) and remain so until the end of February (JD 5935). There is no dramatic drop in mooring temperatures following the onset of shelf upwelling, although the cooler temperatures observed (Figure 6.3.3) may result from a combination of solar heating and inflow of cool upwelled water. The strong upwelling winds on JD 5875 (Figure 6.3.2) coincide with a marked drop in temperature at all moorings and the simple solar cooling model is only able to account for half of the 1.5 ˚C drop in temperature at this time (Figure 6.3.3).

There is evidence that some of the shelf upwelled water is reaching the eastern side of the TFZ. In Figure 6.3.4, we present SST for February 3rd (JD 5877). As can be seen, the gulf waters (warmed by solar heating) are preferentially cooled on the eastern side of the gulf. The path of the upwelled plume follows that from previous studies (eg., Middleton and Bye 2007) and it is possible some upwelled water moves into the TFZ as a sub-surface plume.

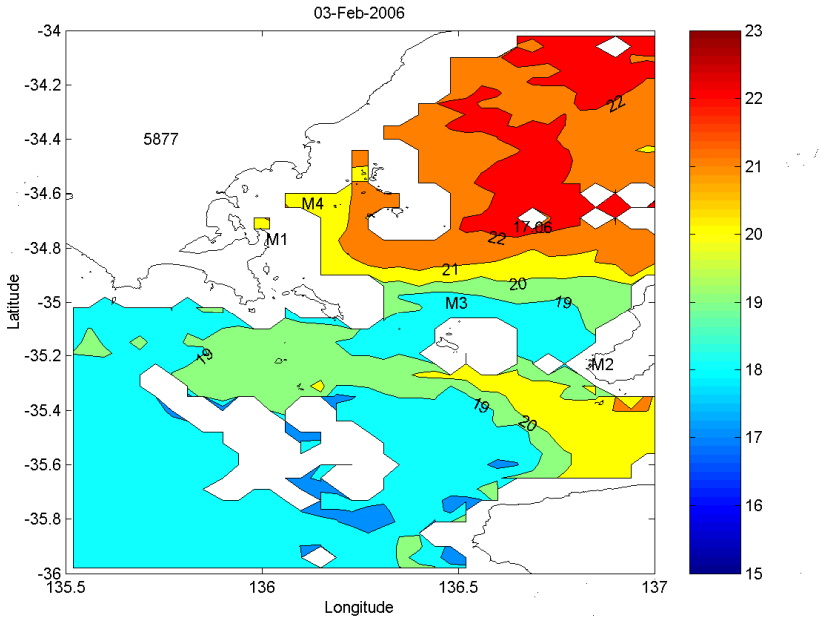

Figure 6.3.4. SST (MODIS) for February 3rd, 2006 (JD 5877).

Transects of temperature and salinity for February 11th 2006 are presented in Figures 6.3.5 and 6.3.6. The transects for temperature provide marginal evidence of upwelling with cooler, fresher water at the bottom and at the eastern side of the transect and close to M4 (boundary). There is also evidence of stratification with a 15 m deep surface mixed layer.

Evidence of evaporation comes from the denser water found on the western transect side that lies in shallower water. This coastal heating and brine water formation is well illustrated in the April 21st 2006 transect shown in Figures 6.3.7 and 6.3.8. The additional salt (0.9 psu) makes the water denser than that offshore with an offshore sub-surface plume structure: the warmest water is at the bottom.

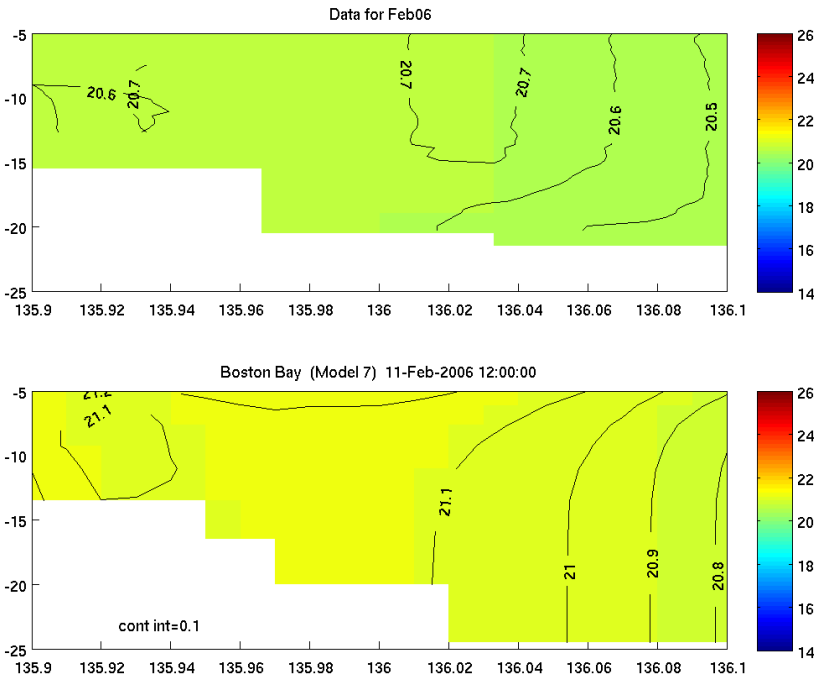

Figure 6.3.5. Upper Panel: observed temperature for February 11th 2006. Lower Panel: model temperature for the same day (12 noon). The vertical scale indicates depths in meters. The horizontal scale is in degrees longitude.

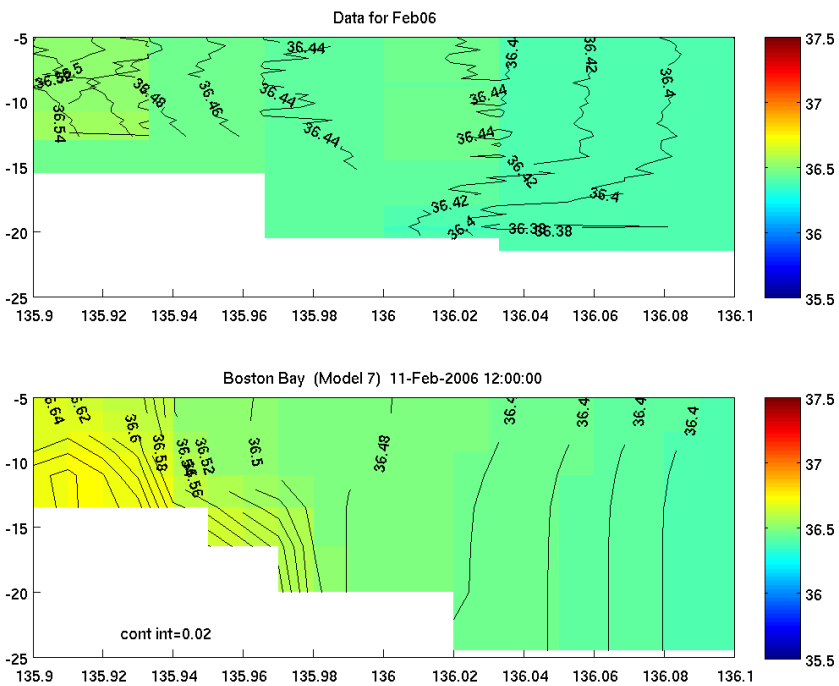

Figure 6.3.6. Upper Panel: observed salinity for February 11th 2006. Lower Panel: model salinity for the same day (12 noon). The vertical scale indicates depths in meters. The horizontal scale is in degrees longitude.

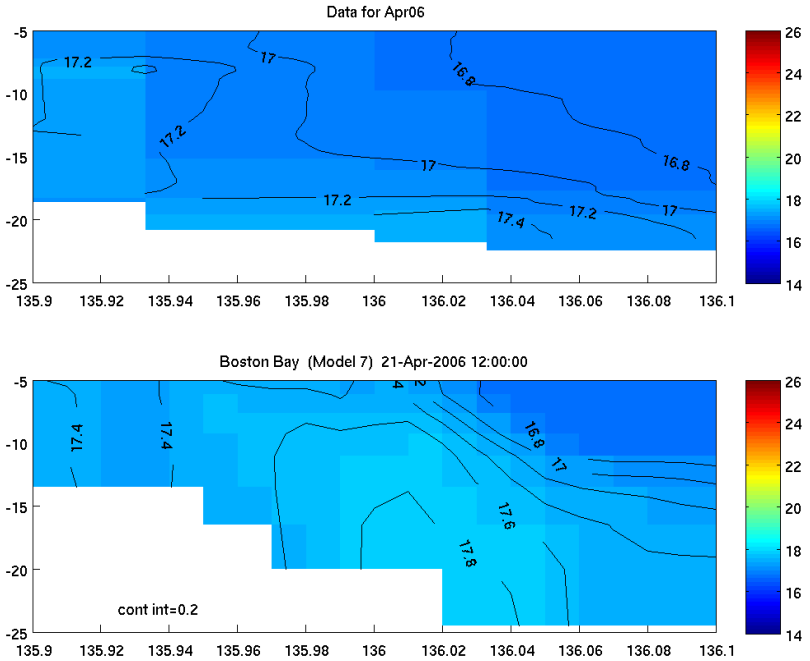

Figure 6.3.7. Upper Panel: observed temperature for April 21st 2006. Lower Panel: model temperature for the same day (12 noon). The vertical scale indicates depths in meters. The horizontal scale is in degrees longitude.

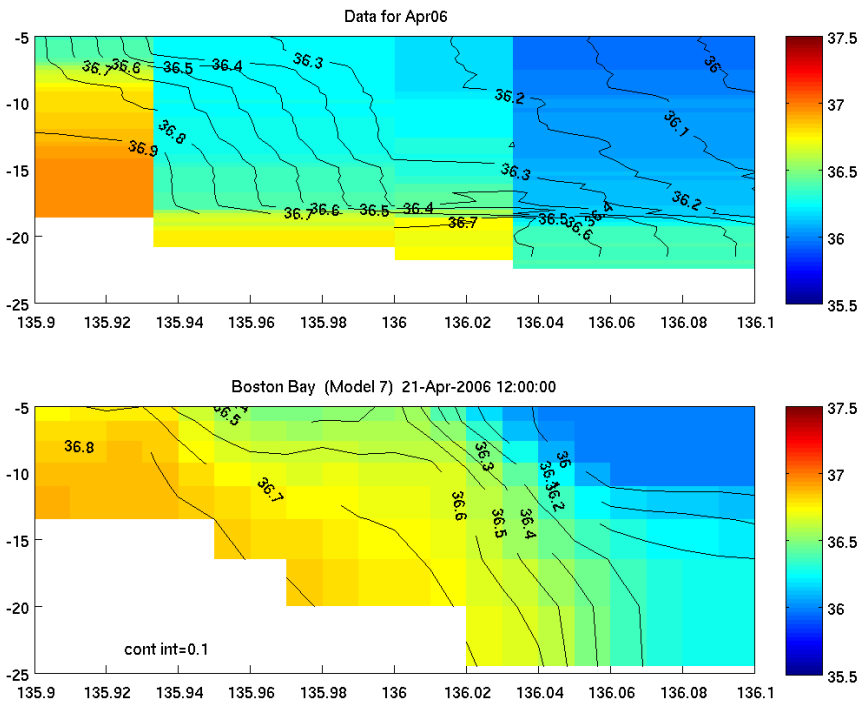

Figure 6.3.8. Upper Panel: observed salinity for April 21st 2006. Lower Panel: model salinity for the same day (12 noon). The vertical scale indicates depths in meters. The horizontal scale is in degrees longitude.

After April, the atmospheric cooling begins to dominate. The transect data for June 20th 2006 are presented in Figures 6.3.9 and 6.3.10 and indicate cold dense water formation at the coast that flows to the east as a 2-3m deep bottom plume. Isotherms near the coast are vertical indicating convective over-turning. Salinity is largely homogeneous.

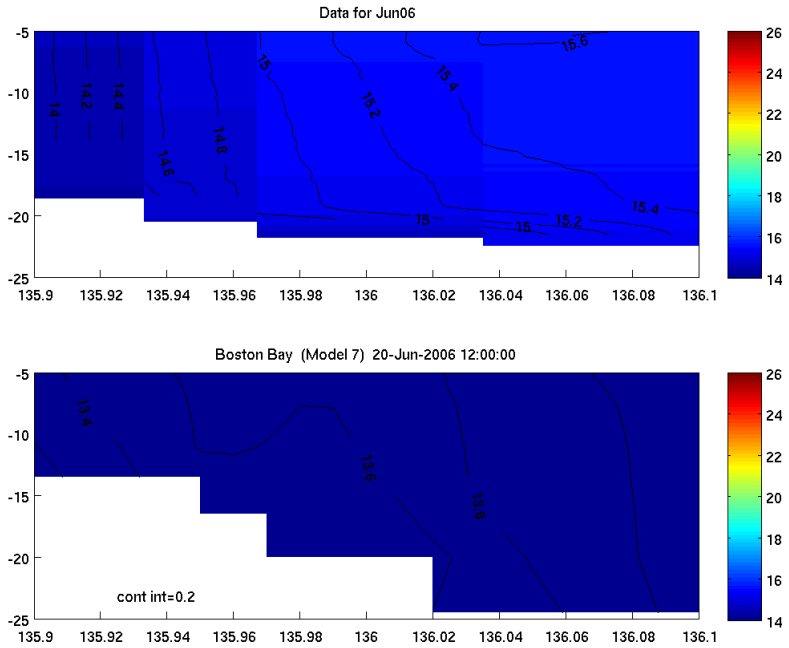

Figure 6.3.9. Upper Panel: observed temperature for June 20th, 2006 (JD 6012). Lower Panel: model temperature for the same day (12 noon). The vertical scale indicates depths in meters. The horizontal scale is in degrees longitude.

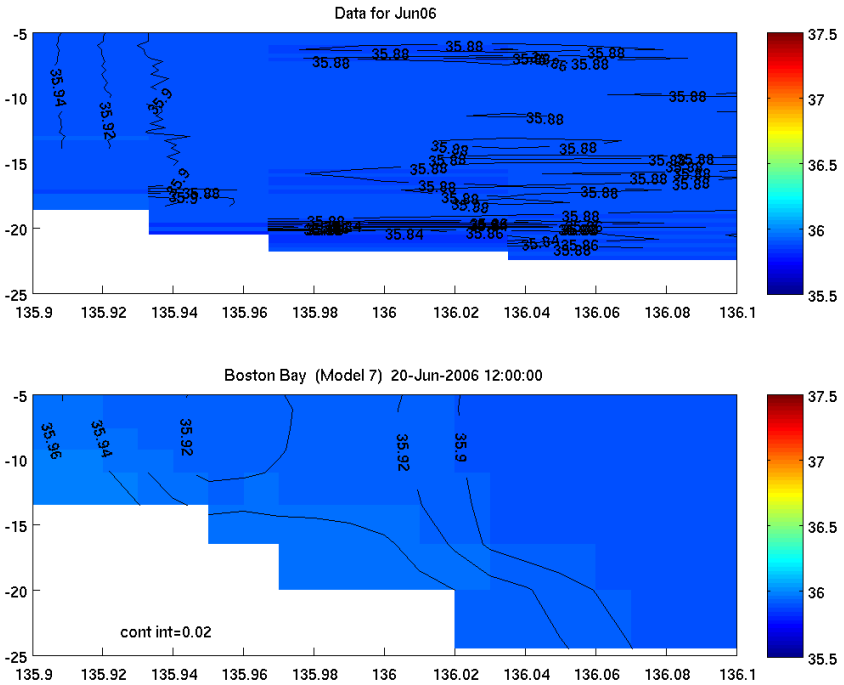

Figure 6.3.10. Upper Panel: observed salinity for June 20th, 2006 (JD 6012). Lower Panel: model salinity for the same day (12 noon). The vertical scale indicates depths in meters. The horizontal scale is in degrees longitude.

The spatial extent of this coastal cooling is illustrated by the SST image (Figures 6.3.11 and 6.3.12). A cyclonic (clockwise) gyre is evident at the large scale as was inferred by Lennon et al (1987).

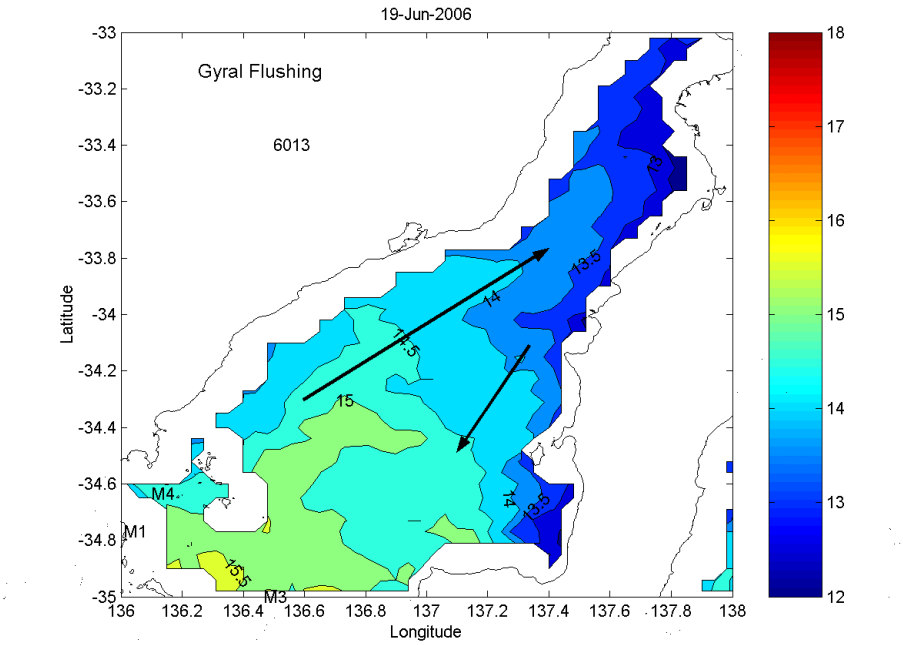

Figure 6.3.11. Sea Surface Temperature (MODIS) for the 19th June 2006(JD 6013). The arrows indicate the expected circulation.

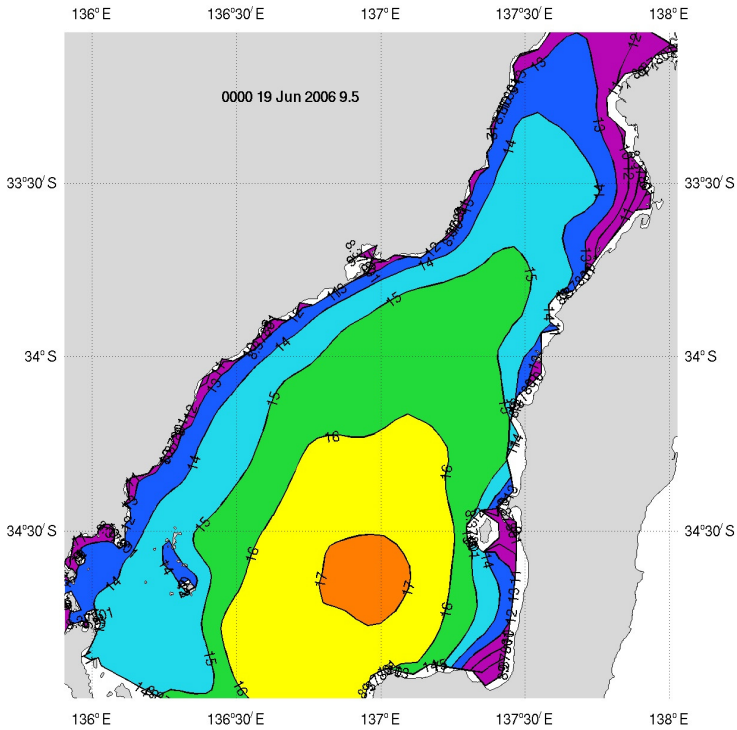

Figure 6.3.12. Modelled Sea Surface Temperature (MODIS) for the 19th June 2006(JD 6013).

6.4. Sea Level Data

The Low-frequency Signals:

Sea level variations are dominated by the tides with amplitudes of up to one meter in the TFZ region (Figure 7.1.1). These will be discussed below. Of interest also is the low-frequency variability that arises from local and remote winds and for periods 3-20 days – the weather-band. While the tides are deterministic (repeatable and predictable), the weather-band signals are less so. Indeed, as we will see, the displacement of fluid parcels that arises from the weather-band circulation exceeds that due to the stronger tidal velocities.

To examine these signals, the sea level data from moorings M4 and M5 were low-pass filtered using the Thompson (1983) algorithm and the results presented in Figure 6.4.1 (the black curves). As can be seen, the signals are dominated by 3-20 day variability with amplitudes of up to 50 cm. Larger variability is found during winter.

Also evident from Figure 6.4.1, is the similarity of sea level signals at the three mooring sites. A similar result is found for the gulf mouth sites. An analysis of the sea level data from moorings M4 and M5 indicates that the geostrophic velocities for the TFZ region are small and less than 5 cm s^{-1} or so. These results will be discussed further in section 6.6 below. For the gulf mouth, differences of 5-10 cm can lead to substantial currents of 20 -30 cm s^{-1}, as discussed next and in Appendix A.

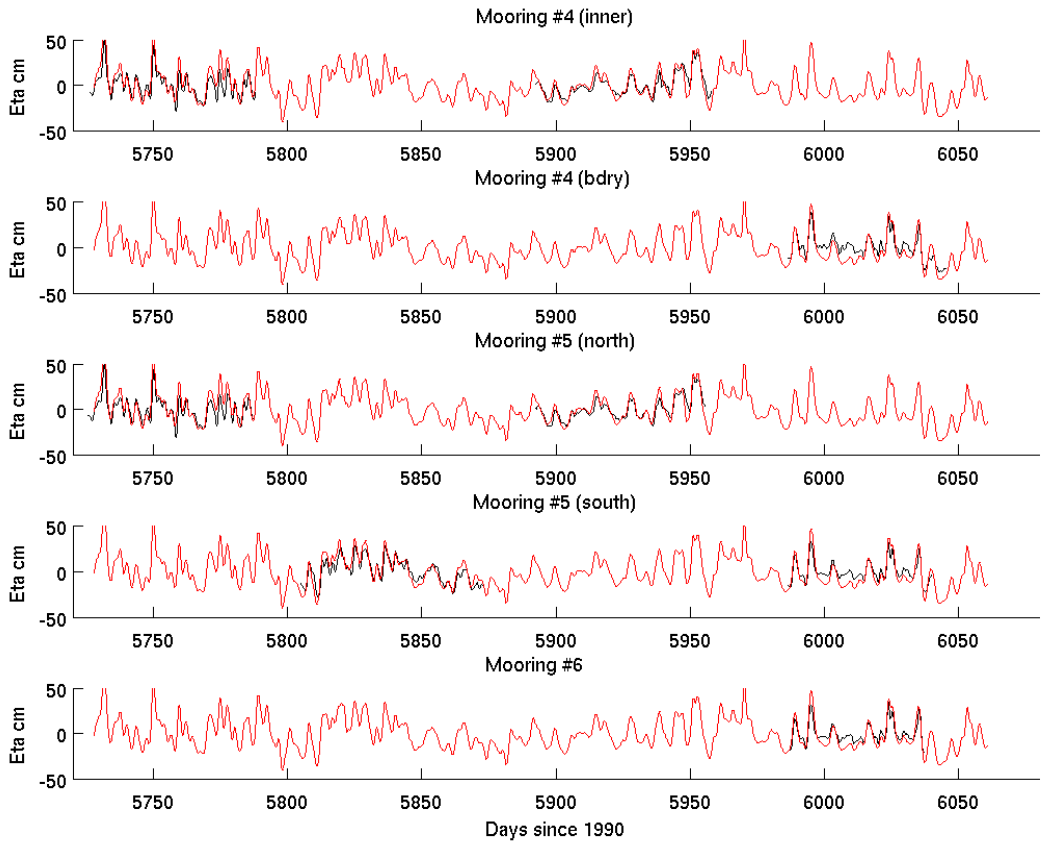

Figure 6.4.1. The low-passed filtered sea level data from the M4, M5 and M6 moorings. Red curve = modelled, black curve = measured.

Circulation at the Gulf Mouth.

As noted, the sea level records from M1 and M2 were found to have datum shifts of 10 –20 cm brought about by re-deployment of the instruments at slightly different depths after servicing (Table 6.1). However, in Appendix A, an analysis of the data suggests a simple conceptual model that likely explains net in/out flows through the gulf mouth that appear to be driven in part by the alongshore wind stress. The data also suggests the existence of anticyclonic (cyclonic) circulation at the gulf mouth during periods of alongshelf upwelling (downwelling) winds. These results are in qualitative agreement with recent numerical studies elsewhere (Middleton and Teixeira 2008).

6.5. Velocity Mooring Data

Hourly averages of velocity data from bottom mounted ADCPs at moorings M4 and M5 were calculated. For M4, currents were measured in 69 bins (each of 0.5 m depth) from the bottom (offset for instrument blanking and mooring infrastructure) to the surface. For M5, currents were measured in 24 (0.5m depth) bins but only from the bottom to 12 m above the sea floor. Note that both moorings were shifted to different sites for the 2nd and 4th deployments (see Figure 6.1.2).

Depth-Averaged Velocities.

As a first step, the data was averaged in the vertical and the Thompson (1983) filter applied. With the filtered data so determined, residual (tidal band) time series were then obtained: simply the residual data being the raw data less the filtered data. Plots of the tidal band signals are presented in Figure 6.5.1 for the M4 inner site. Results for the M4 boundary site are similar. Results for M5 (not shown) are similar but reduced in magnitude to 5-10 cm s^{-1}.

For the east/west and north/south components presented in Figure 6.5.1, it is evident that the latter dominate with speeds of 30 cm s^{-1}. The fortnightly dodge tide is also evident.

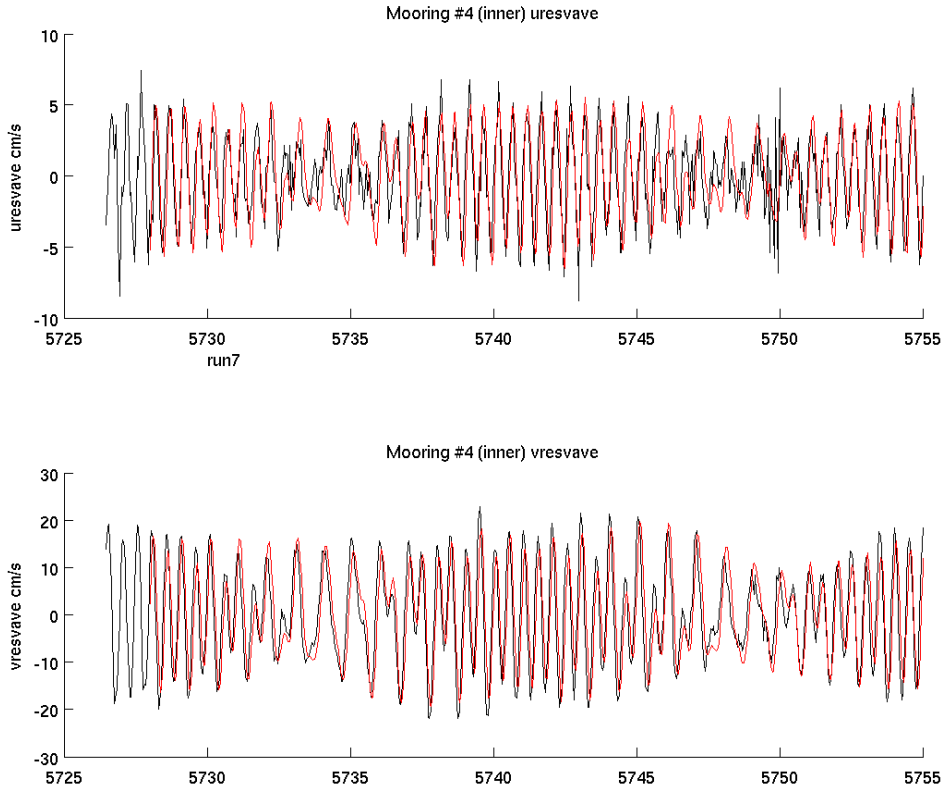

Figure 6.5.1. Upper Panel: the (east/west) tidal-band velocity (depth-averaged) for the M4 inner site. Black values are data while the red values are from the fine scale numerical model. Positive values are to the east. Lower Panel: as in the upper panel but for the (north/south) tidal-band velocity. Positive values are to the north. Note the change of limits on the y- axis.

The filtered depth-averaged velocity field is shown in Figure 6.5.2, again for the inner sites. As is evident, there is again variability in the 2-30 day band. Strikingly, the current speeds of the filtered (weather-band) data are much smaller (< 5 cm s^{-1}) than those of the tides (~ 30 cm s^{-1}) shown in Figure 6.5.1. The small current speeds are, however, consistent with geostrophic currents estimated from the M4 and M5 sea level data.

Results were also obtained for the other sites (including M5) and were similar in character to those shown in Figures 6.5.1-6.5.2, with amplitudes 5 cm s^{-1} or less.

The weather-band currents within the gulf are much smaller than those typically found on the shelf (~ 25 cm s^{-1}). The reason for this is that the coastal boundary conditions of no normal flow penetrate over a distance of the deformation radius which is around 120 km and comparable to the gulf width (Middleton and Teixeira 2008). These authors have also shown that larger weather-band currents will be found in very shallow water (< 5 m), since the deformation radius is effectively smaller.

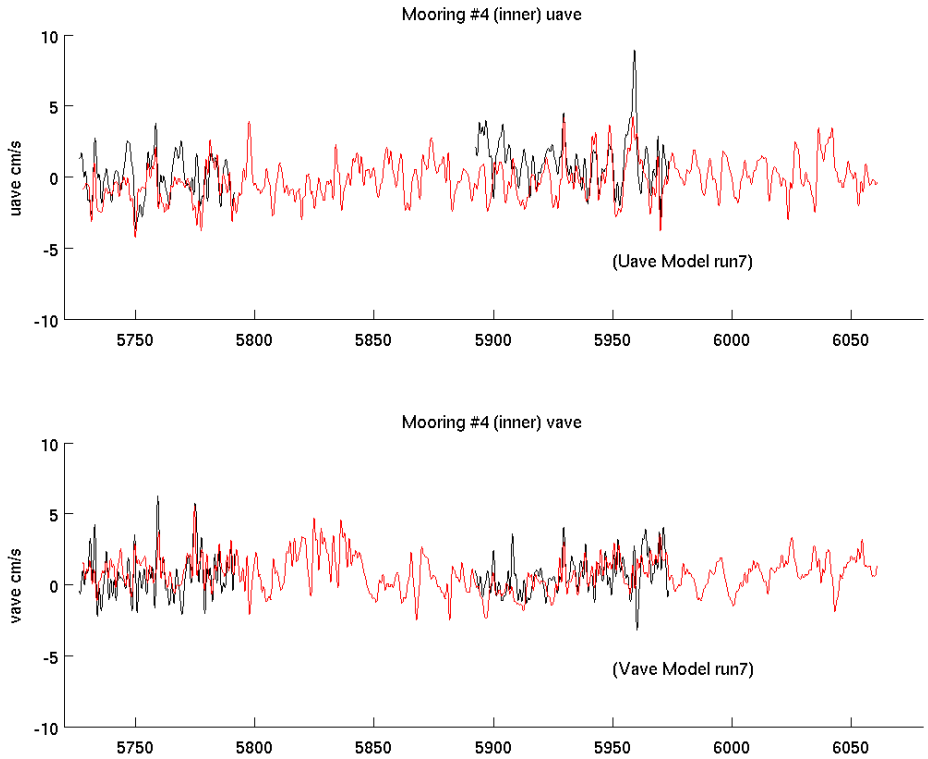

Figure 6.5.2. Upper Panel: the (east/west) weather-band velocity (depth-averaged) for M4 at the inner site. Black values are data while the red values are from the fine scale numerical model. Positive values are to the east. Lower Panel: as in the upper panel but for the (north/south) weather-band velocity. Positive values are to the north.

The stronger semi-diurnal tidal currents shown in Figure 6.5.1 may be implicated in bottom stirring, particularly when wave action is included. A useful measure of their importance to flushing is the net displacement a water parcel would undergo after ¼ period (3 hrs). For the dominant semi-diurnal tide this distance is 1.4 km. For the weaker weather-band currents, the displacements will generally be larger since they persist over a longer time. For example, a 5 cm s^{-1} current with a 10 day period will displace a water parcel by 7 km over a 2.5 day period: five times that of the tide. Thus, the successful modelling of the low-frequency circulation may be more important to predicting cage flushing and nutrient transport than that of the tides.

Mean Currents and Velocity Shear.

The above presents results for the depth-averaged currents. The mean currents may be important to flushing. In addition, vertical current shear may be important to enhanced shear dispersion and also lead to modifications to bottom stirring and flushing through the cages themselves. To this end, we have calculated statistics for the mean currents, shear and deflections (Appendix C).

Means: In summary, the results for M4 show the mean flow to be small (~ 1 cm s^{-1}) and directed to the north-east for most of the year (Appendix C). Such a flow will displace a fluid parcel by 78 km over a 3-month seasonal period. For M5, the mean flow is predominantly to the south or west with speeds of 2-3 cm s^{-1}, i.e. an onshore flow.

Shear: Shear statistics were calculated for the raw, filtered (weather-band) and tidal band components of the flow. The currents in the bottom ADCP bin (~ 1m from the bottom) for M4 were found to be deflected to the left of the depth-averaged currents - an indication of Ekman dynamics. Indeed the results in Appendix C suggest that frictional boundary layer dynamics are important at both the surface and bottom. In summary, the statistics of the depth-averaged velocities ($\bar{u}, \bar{v}$) for M4 are given in Table 6.2 for each deployment period (D=1, 2, 3 or 4).

Table 6.2. $\sqrt{<\bar{u}^2>}, \sqrt{<\bar{v}^2>}$: rms of depth-mean velocity components at M4. The braces <> denote a time average for the given deployment period.

	Unfiltered				Low Frequency				Tidal Band			
D	1	2	3	4	1	2	3	4	1	2	3	4
u	3.3	3.1	3.7	3.4	1.4	1.8	2.0	1.7	2.9	2.5	3.1	3.0
v	10.8	10.0	10.9	12.7	1.7	1.5	1.4	2.6	10.7	9.9	10.8	12.4

D: Deployment; *u* and *v* in cm s^{-1}

For the unfiltered data, the rms (root mean square) variability is largest in the north/south direction and largely accounted for by the tides. Now consider the rms shear statistic:

$$\sigma^u{}_z(t) = \sqrt{\frac{1}{h}\int_{-h}^{0}(u-\bar{u})^2\,dz}$$

(and similarly for *v* component) and its time average: $<\sigma^u{}_z(t)>$. Results for the later statistic are shown in Table 6.3.

Table 6.3. $<\sigma_z^u(t)>, <\sigma_z^v(t)>$: time averages of standard deviations along z-axis at M4.

	Unfiltered				Low Frequency				Tidal Band			
D	1	2	3	4	1	2	3	4	1	2	3	4
u	5.0	21.7	7.1	10.6	1.7	2.6	3.4	3.9	4.2	4.9	5.9	3.8
v	11.3	37.6	11.1	23.7	1.6	1.3	1.4	1.8	14.6	13.8	16.3	10.9

D: Deployment; *u* and *v* in cm s^{-1}

The results show that the rms shear is as large as or larger than the variability of the depth-averaged velocities in Table 6.2 for the raw, filtered and tidal band signals.

For M5, the results show the rms depth averaged variability to be much smaller in the tidal band (~ 3-5 cm s^{-1}), although the shear is again comparable to this average (Appendix C).

Finally, we consider a progressive vector diagram (pvd) using the filtered data from the M4 site and second deployment period that covers the wintertime wind conditions (predominantly from the west) to summertime upwelling conditions (predominantly from the south-east). The pvd is a vector plot of the distance a fluid parcel would travel assuming its velocity is given by the (fixed point) mooring (or wind) data.

The pvd in Figure 6.5.3 shows the surface currents starting at zero displacement in x and y on 6th December 2005 (JD 5818 in the figure) and proceeding to 3rd February 2006 (JD 5877).

The surface flow was generally to the north or northeast throughout the summer period, with no pronounced change in direction during the deployment period.

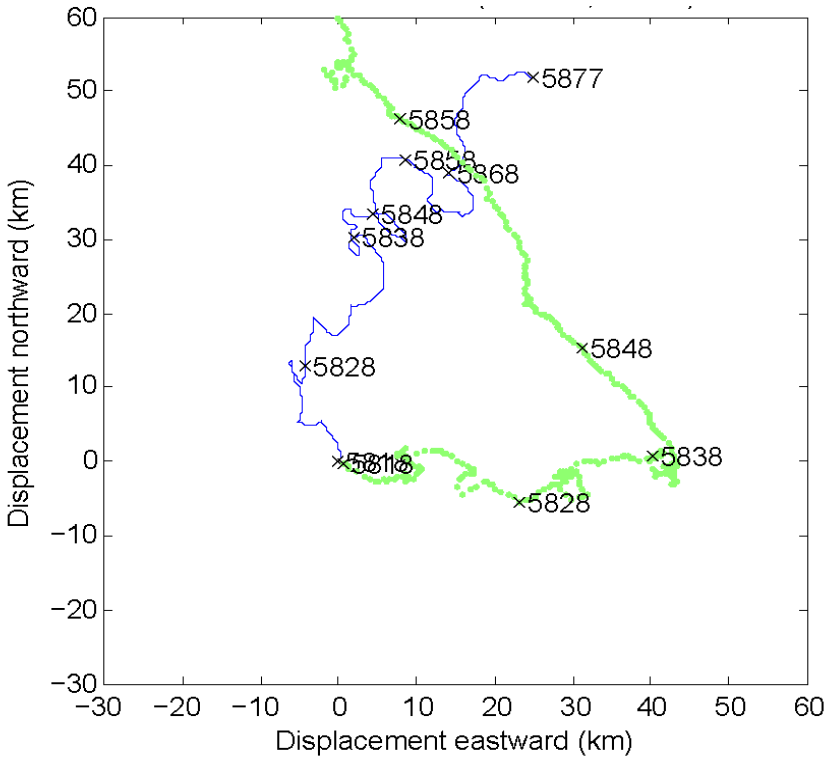

Figure 6.5.3. Progressive Vector Diagram of near-surface currents at Mooring 4 (blue line). The green line is the predicted "surface drift" based on 2% of the local winds. The times are in Julian Days since 1990. and begin (JD5818) on December 6th 2008.

The surface drift shown is that based on a simple empirical formula, which states that the water within a meter or two of the surface moves in nearly the same direction as the wind, at approximately 2% of the wind speed. Essentially, it gives an integrated measure of the wind and direction. Over the first 22 days, the winds are directed to the east. At JD 5838 (December 28th), the winds shift to become directed to the north-west and are typical of those for summer (shelf upwelling). Paradoxically, the surface currents are directed to the north/north-east and remain so regardless of the wind direction.

The flow at the bottom (Figure 6.5.4) is to the northwest for the first 20 days and approximately opposite to the direction of the winds. That is an onshore (local upwelling) flow is found. As the winds change direction, so does the bottom current, becoming directed to the east and more or less in the opposite direction to the surface winds: local downwelling.

These results (and those above for the CTD transects) indicate that the shear in the oceanic velocity field can be large and that local winds can lead to on/offshore flows and associated upwelling and downwelling. The model results will illustrate this further below.

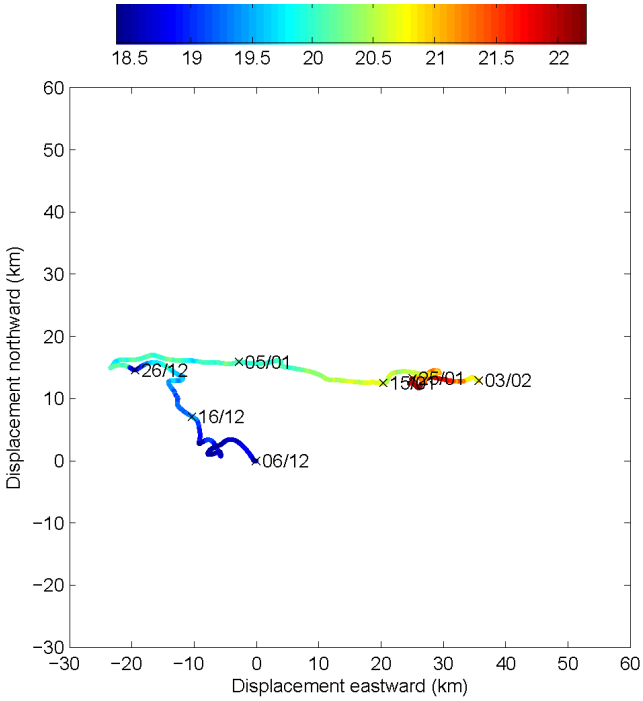

Figure 6.5.4. Progressive vector diagram of near-bottom currents at Mooring 4. The times (December 2006 - January 2006) are indicated by dd/mm. The colour gives the near-bottom temperature from the M5 mooring at the dates indicated: colour bar at top of figure